

## Early Paleozoic Granitoid Magmatism in the East Tannu-Ola Sector of the Tuvinian Magmatic Belt: Geodynamic Setting, Age, and Metallogeny

E.V. Vetrov<sup>a,b,✉</sup>, A.I. Chernykh<sup>c</sup>, G.A. Babin<sup>a,d</sup>

<sup>a</sup> Siberian Research Institute of Geology, Geophysics and Mineral Resources, Krasnyi pr. 67, Novosibirsk, 630091, Russia

<sup>b</sup> V.S. Sobolev Institute of Geology and Mineralogy, Siberian Branch of the Russian Academy of Sciences,  
pr. Koptyuga 3, Novosibirsk, 630090, Russia

<sup>c</sup> Central Research Institute of Geological Prospecting for Base and Precious Metals, Varshavskoe shosse 129, korp. 1, Moscow, 117545, Russia

<sup>d</sup> A.P. Karapinsky Russian Geological Research Institute, Srednii pr. 7, St. Petersburg, 199026, Russia

Received 22 November 2017; received in revised form 6 August 2018; accepted 17 September 2018

**Abstract**—The East Tannu-Ola sector of the Tuvinian magmatic belt is composed of Early Cambrian volcanosedimentary rocks of an island-arc association (Kadvoi, Serlig, and Irbitei Formations), which are intruded by granitoid massifs of different ages (from Cambrian to Devonian) of the Tannu-Ola areal pluton. We analyzed the structural and geologic position, chemical composition, metallogenic signatures, and geochronological (U/Pb) and isotope-geochemical (Sm/Nd and Rb/Sr) characteristics of Early Paleozoic granitoids of the Ungesh pluton (western part of the Tannu-Ola areal pluton). The available and our new data made it possible to establish the specific chemical parameters, age sequence, duration, intensity, and metallogeny of granitoid magmatism in the East Tannu-Ola sector of the Tuvinian magmatic belt. An early Cambrian (534–518 Ma) gabbro–plagiogranite complex similar to the Maina complex in West Sayan has been recognized in the Ungesh pluton. The age and metallogeny of the middle–late Cambrian (508–492 Ma) Tannu-Ola diorite–granodiorite–plagiogranite and Late Ordovician (451–447 Ma) Argolik granite–leucogranite complexes have been refined. Granitoids of the early Cambrian complex formed probably at the initial stage of formation of an island arc, in association with the Kadvoi–Serlig basalt–andesite–rhyolite complex. It is in these granitoids that early low-productivity gold–sulfide–quartz veins and veinlets originated. Granitoids of the Tannu-Ola complex formed at the initial stage of evolution of the accretion–collision system. Magnetite-containing skarns and numerous vein–veinlet zones of late high-productivity gold–sulfide–quartz mineralization evolved in these granitoids. Granitoid massifs of the Argolik complex formed at the final stage of evolution of the accretion–collision system and probably played a crucial role in the regeneration of ore mineralization in some areas.

**Keywords:** granitoid magmatism, U/Pb (SHRIMP-II) zircon dating, petrogeochemical and isotope-geochemical (Sm/Nd and Rb/Sr) studies, gold, copper, lead, zinc, metallogeny, Republic of Tyva, East Tannu-Ola sector, Tuvinian magmatic belt

### INTRODUCTION

In the East Tannu-Ola sector of the Tuvinian magmatic belt, massifs of the middle Cambrian Tannu-Ola diorite–granodiorite–plagiogranite and Early Devonian Bren’ granosyenite–granite–leucogranite complexes were commonly recognized (Pinus, 1961; Ivanova, 1963; Teleshev, 1981; Shapovalov, 2001). The rock appearance played a significant role for the division of granitoids of the East Tannu-Ola sector. For example, grayish-red leucocratic granites were usually assigned to the Early Devonian Bren’ complex, and gray plagiogranites, to the middle Cambrian Tannu-Ola complex. Recent studies by precision methods have shown that the Tannu-Ola areal pluton, along with other granitoid areal plutons in Tuva (Kaa-Khem, Khamsara, Bii-Khem, etc., Fig. 1), has a heterogeneous and polychronous structure

and an age of 450 to 570 Ma (Rudnev et al., 2004, 2005, 2006, 2015; Rudnev, 2013).

The polychronous magmatism of different compositions in the East Tannu-Ola sector of the Tuvinian magmatic belt is responsible for diverse endogenous mineralization of different ages. The East Tannu-Ola ore district is confined to the field of rocks of the Tannu-Ola areal pluton breaking through the early Cambrian volcanosedimentary rocks of the Kadvoi–Serlig complex. It has prospecting indicators of gold, gold-bearing polymetallic (Cu, Pb, Zn, Au, and Ag), copper, iron, and molybdenum types of mineralization (Chernykh, 2014; Chernykh et al., 2017). Thus, division of the Tannu-Ola areal pluton into sectors and study of their geology, chemical composition, and age will help not only to elucidate the evolution and the model of formation of granitoid magmatism but also to clarify the spatial and temporal distribution of minerals and the parameters of the relationship of Au and porphyry Mo–Cu types of mineralization with intrusive complexes.

<sup>✉</sup> Corresponding author.

E-mail address: vetrovggdnnsu@yandex.ru,  
vetrov@igm.nsu (E.V. Vetrov)

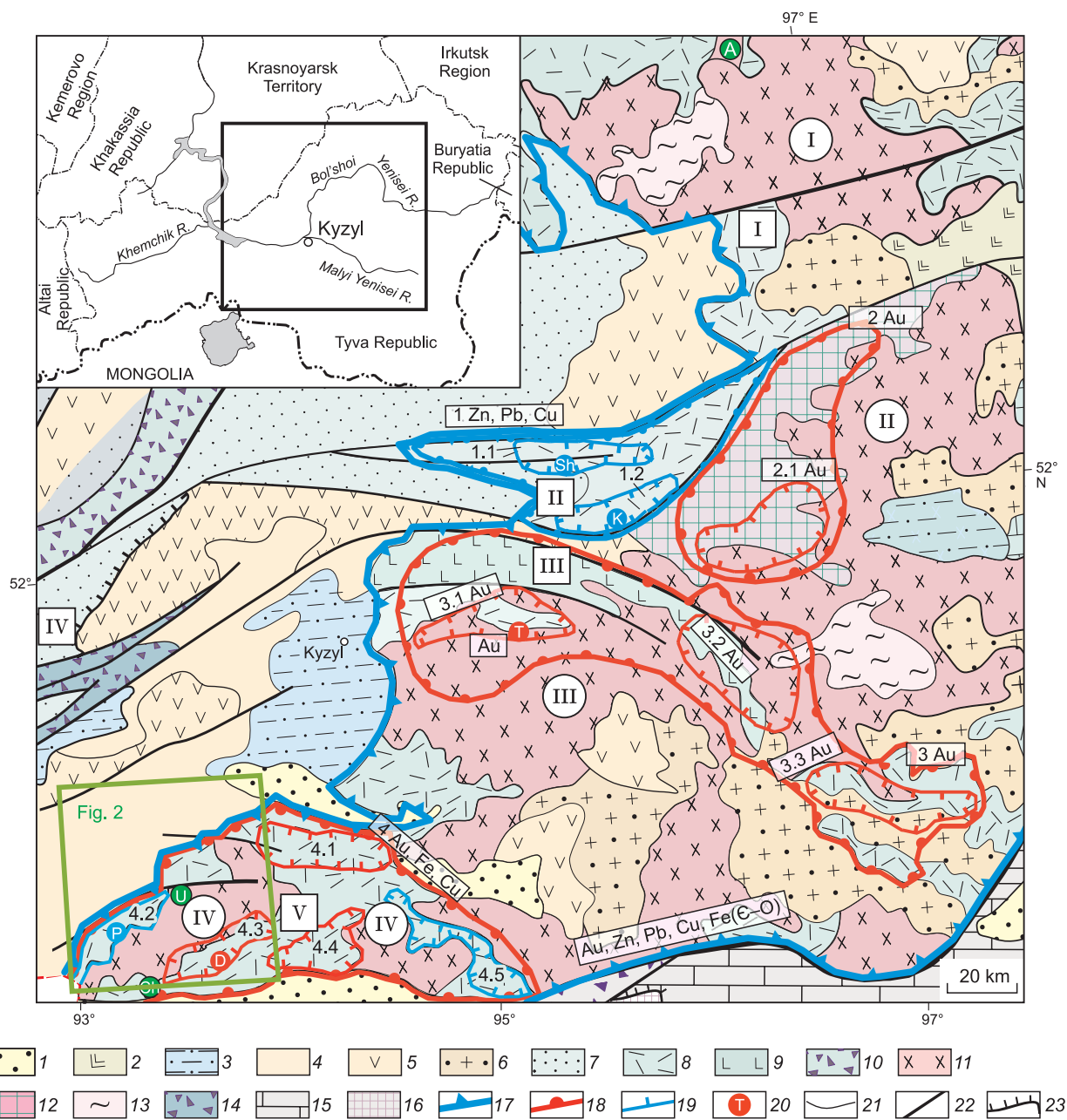


**Fig. 1.** Geological schematic map of the Tuvinian magmatic belt. 1, Cenozoic depressions; 2, Cenozoic East Tuva volcanic basaltic plateau; 3, Jurassic depressions; 4, Middle Paleozoic terrigenous deposits; 5, Middle Paleozoic differentiated medium-alkali rock complex; 6, Middle Paleozoic granosyenite-granite and nepheline-syenite rock complexes; 7, carbonate terrigenous deposits of passive margin (O–S); 8, Ediacaran(?)–Cambrian deposits of basalt-plagioclase complex; 9, Ediacaran(?)–Cambrian volcanosedimentary deposits with basalts and ultrabasites; 10, Ediacaran(?)–Cambrian melanges; 11, Cambrian–Ordovician granitoids; 12, blocks of Late Riphean(?) basement (areas of early Paleozoic green-schist metamorphism); 13, blocks of Tonian(?) basement (epidote–amphibolites and amphibolite complexes); 14, Ediacaran–Cambrian ophiolite association; 15, carbonate deposits of the Ediacaran–Cambrian nappe; 16, uplifts of Tonian metamorphic basement; 17–19, borders of metallogenic units; 17, Tannu-Ola–Ulugoi Fe–Cu–Au–polymetallic mineralization zone, 18, ore districts, 19, ore clusters; 20, mineral deposits and ore occurrences; 21, geologic boundaries; 22, tectonic boundaries; 23, thrusts.

Metallogenic units: Tannu-Ola–Ulugoi Fe–Cu–Au–polymetallic mineralization zone: 1 Zn, Pb, Cu, Kyzyl-Tash deposit; 1.1, Kyzyl-Tash pyrite–polymetallic ore district; 1.2, Kyzyl-Tash pyrite–polymetallic ore cluster; 2, Kharal gold ore/gold placer district; 2.1, Kharal (Mozgolev) gold ore/gold placer cluster; 3, Tapsa-Kaa-Khem gold ore/gold placer district; 3.1, Tardan gold ore/gold placer cluster; 3.2, Kagzhirba–Kundus gold ore/gold placer cluster; 3.3, Karabil'dyr gold ore/gold placer cluster; 4, East Tannu-Ola Cu–Fe–Au–polymetallic ore district; 4.1, Elegest–Mezhegei gold ore/gold placer cluster; 4.2, Irbitei Au–Ag–polymetallic ore cluster; 4.3, Aptara gold ore cluster; 4.4, Shivilig gold ore cluster; 4.5, Shivilig–Khem Au–Ag–polymetallic ore cluster. Sectors of the Tuvinian magmatic belt (in squares): I, Khamsara; II, Kaa-Khem; III, Ulugoi; IV, Uyuk; V, East Tannu-Ola. Granitoid areal plutons (in circles): I, Khamsara; II, Bii-Khem; III, Kaa-Khem; IV, Tannu-Ola. Deposits and ore occurrences: gold: T, Tardan deposit; D, Despen ore occurrence; polymetallic: KT, Kyzyl-Tash ore occurrence; K, Kyzyl-Tash deposit; P, Podpereval'noe ore occurrence; porphyry Mo–Cu: A, Ak-Sug Au-containing deposit; U, Ulug-Sailyg ore occurrence; Ch, Ak-Chary ore occurrence.

In this paper we present results of comprehensive studies of granitoids in the west of the Tannu-Ola areal pluton (Ungesh pluton), carried out within the framework of the GDP-200 (“Additional geological study of areas” project) research in the area covered by Sheet M-46-X (Khovu-Aksy region) of the Geological Map of the Russian Federation. During these studies, the granites of the Ungesh pluton were divided into complexes, and their geologic structure, age, petrogeochemical composition, isotope (Sm/Nd and Rb/Sr) characteristics, and metallogeny were studied in detail. Based on the new data, we analyzed the age sequence and duration of intrusion and the conditions of generation of parental melts at different geodynamic stages of the regional evolution. We also refined the specifics of the regional metallogeny and established the main stages of its formation.

## METHODS

The early Paleozoic granitoids of the Ungesh polychronous pluton were studied by a complex of methods, including analysis of cartographic materials, field observations, and petrographic, petrogeochemical, isotope-geochronological, and isotope-geochemical studies.

Based on the direct field observations, we divided the Early Paleozoic granitoids of the Ungesh pluton into complexes, mapped them, studied their structure, composition, and metallogenic specialization, recognized the intrusion phases, and investigated the relationships between these phases and the host rocks and between different types of granitoids.

Petrographic and analytical laboratory studies gave an insight into the microcomposition of the recognized rock varieties. During the petrographic study of slices, special attention was paid to the mineral composition, structures and textures of rocks, and the set of accessory minerals.

Analysis for petrochemical elements was performed on an ARL Optim’X X-ray fluorescence spectrometer (Germany) in the laboratory of the Siberian Research Institute of Geology, Geophysics and Mineral Resources (SNIIGGiMS), Novosibirsk (analyst D.O Artomonov), following the NSAM 439-RS technique with measurement of the intensities of X-ray fluorescence of the elements under study and their comparison with the intensities of standard samples.

The contents of rare-earth elements (REE) and trace elements were determined with an ELAN-DRC-6100 (USA) ICP mass spectrometer in the Central Laboratory of the Russian Geological Research Institute (VSEGEI), St. Petersburg (analysts V.A. Shishlov and V.L. Kudryashov).

The age of intrusive complexes was estimated by U/Pb (SHRIMP-II) dating of granitoids at the Center of Isotopic Research (CIR) of VSEGEI (analysts A.N. Larionov and E.N. Lepekhina), following a standard technique (Williams, 1998) with the use of the TEMORA standard (Black et al., 2003). The error of single analyses is at the  $1\sigma$  level, and the error of calculation of the concordant age is at the  $2\sigma$  level.

Concordia diagrams were constructed using the Isoplot/Ex program (Ludwig, 2003).

The sources of magma-forming substrates for the dated granitoids of different complexes were assessed based on the Rb/Sr and Sm/Nd isotope-geochemical characteristics of their bulk samples (CIR VSEGEI, St. Petersburg). Analysis of Sm, Nd, Rb, and Sr isotopes was performed on a Triton T1 seven-collector mass spectrometer, following the earlier proposed techniques (Bogomolov et al., 2002). The accuracy of Sr and Nd isotope measurements was controlled by analysis of the VNIIM-Sr ( $^{87}\text{Sr}/^{86}\text{Sr} = 0.70801 \pm 20$ ) and INd-1 ( $^{143}\text{Nd}/^{144}\text{Nd} = 0.5121003 \pm 104$ ) standards. The  $^{87}\text{Rb}/^{86}\text{Sr}$  and  $^{147}\text{Sm}/^{144}\text{Nd}$  values were calculated from the contents of Rb, Sr, Sm, and Nd determined by ICP MS. The  $\varepsilon_{\text{Nd}}$  and  $(^{87}\text{Sr}/^{86}\text{Sr})_0$  values were calculated relative to the CHUR model chondrite reservoir with  $^{143}\text{Nd}/^{144}\text{Nd} = 0.512638$ ,  $^{147}\text{Sm}/^{144}\text{Nd} = 0.1967$ ,  $^{87}\text{Rb}/^{86}\text{Sr} = 0.7045$ , and  $^{87}\text{Sr}/^{86}\text{Sr} = 0.0816$  (Faure, 1986). The model  $T_{\text{Nd}}$  ages of crustal material were estimated using a two-stage model (Liew and Hofmann, 1988) and parameters  $^{143}\text{Nd}/^{144}\text{Nd} = 0.513079$ ,  $\varepsilon_{\text{Nd}} = 8.6$ , and  $\text{Sm/Nd} = 0.352$  ( $^{147}\text{Sm}/^{144}\text{Nd} = 0.21194$ ) (De Paolo et al., 1991).

## GEOLOGIC STRUCTURE OF THE UNGESH PLUTON

The Ungesh pluton forms the largest body in the west of the Tannu-Ola areal pluton (Fig. 1). It is arched and extends in the E–W direction conformably with the main geologic structures. Outcrops of early Paleozoic igneous rocks of the pluton and its satellites at the recent denudation level are about  $1000 \text{ km}^2$  in area. The Ungesh pluton is hosted by early Cambrian volcanosedimentary rocks of an island-arc association (Kadvoi, Serlig, and Irbitei Formations) (Shapovalov, 2001; Chernykh et al., 2017). The Kadvoi and Serlig Formations are composed of carbonate, volcanic, and terrigenous deposits of basalt–andesite–plagioryholite association, which accumulated at the initial early Cambrian stage of evolution of ensimatic volcanic arcs of the Altai–Sayan system. The Irbitei Formation is made up of terrigenous and carbonate deposits with interbeds of volcanic rocks of basalt–andesite association, which formed at the final stage of evolution of an early Cambrian island arc (Babin et al., 2006).

The Ungesh pluton is composed of rocks of three complexes of different ages: conceivably, Maina-type ( $\mathbb{C}_1$ ) gabbro–plagiogranite (similar to the Maina complex in West Sayan), Tannu-Ola ( $\mathbb{C}_{2-3}$ ) diorite–granodiorite–plagiogranite, and Argolik (O) granite–leucogranite (Fig. 2).

**The Maina-type two-phase gabbro–plagiogranite complex** was recognized tentatively. The first phase is hornblende and quartz gabbro forming separate small elongate bodies of irregular shape, which break through the rocks of the Serlig Formation and the outliers among the granitoids of the Tannu-Ola complex. The second phase is hornblende and hornblende–biotite diorites, granodiorites, plagiogra-

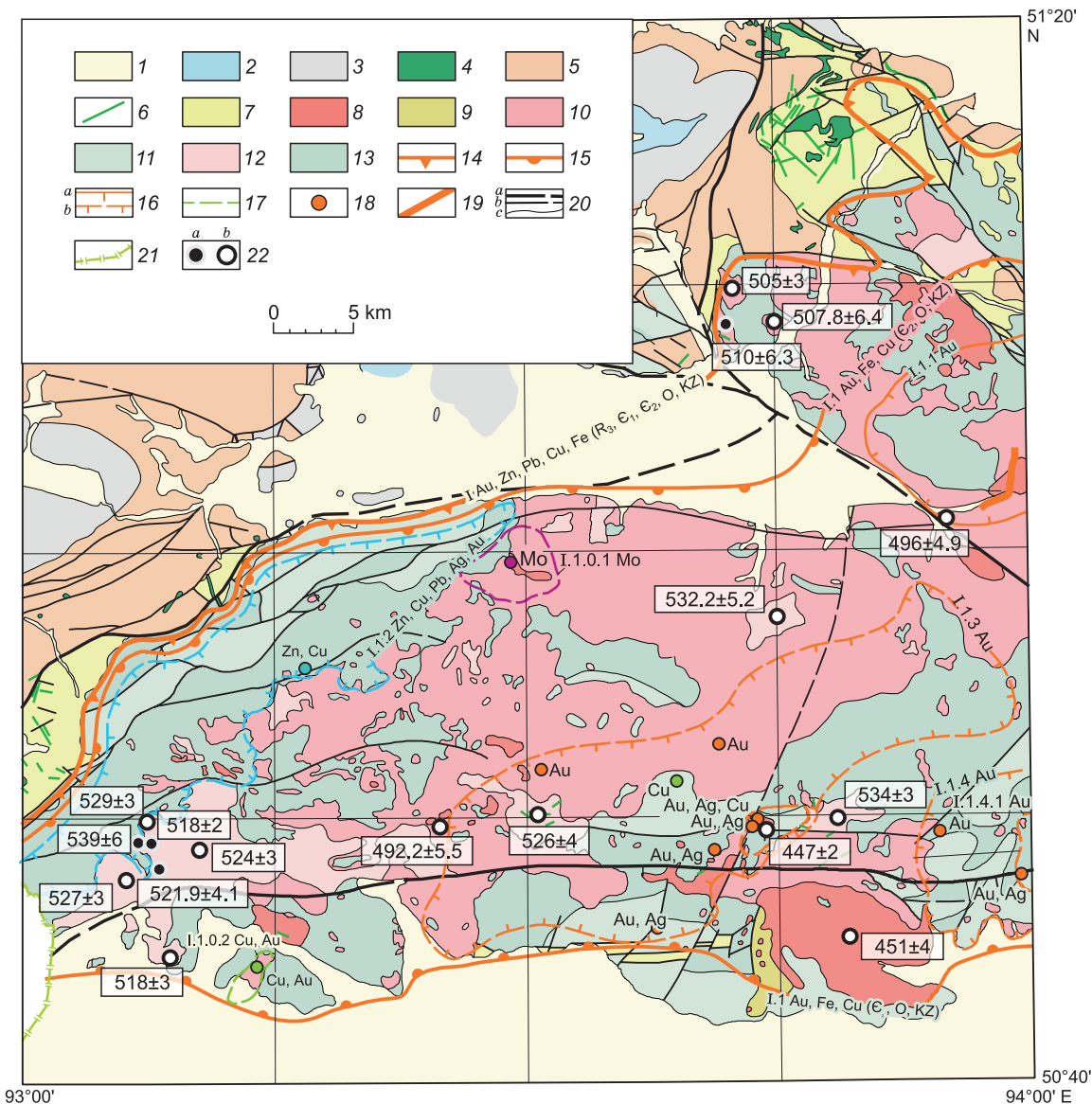


**Fig. 2.** Schematic geologic structure of the western part of the East Tannu-Ola areal pluton (compiled after (Chernykh et al., 2017) and supplemented). 1, Cenozoic deposits; 2, Jurassic coal-bearing molassa; 3, Carboniferous terrigenous rocks; 4, Torgalyg syenite–gabbro complex ( $D_3$ – $C_1$ ); 5, Devonian volcanosedimentary, terrigenous, and terrigenous carbonate deposits of the Central Tuva trough ( $D_1$ – $D_3$ ); 6, basic dikes ( $PZ$ –MZ); 7, Ordovician–Silurian terrigenous and terrigenous carbonate deposits of the Central Tuva trough ( $O_3$ – $S_2$ ); 8, Argolik granodiorite–granite complex; 9, Despen andesite–rhyodacite unit ( $O_3$ ); 10, Tannu-Ola gabbro–diorite–granodiorite–plagiogranite complex ( $\epsilon_{2-3}$ ); 11, Irbitei Formation ( $\epsilon_1$ ); 12, Maina-type gabbro–plagiogranite complex ( $\epsilon_1$ ); 13, united Kadvoi and Serlig Formations; 14–17, borders of metallogenic units: 14, metallogenic zones, 15, ore districts, 16, ore clusters (a) and predicted ore clusters (b), 17, predicted ore fields; 18, ore occurrences with metallogenic signatures (Au, gold, Cu, copper, Mo, molybdenum, Zn, zinc, Ag, silver); 19, small deposit of placer gold; 20, boundaries (a, major faults, b, subsidiary faults, c, between geologic units); 21, Russia–Mongolia state border; 22, locality of sampling for isotope dating (a, published dates, b, new dates, Ma).

Metallogenic units: I, Tannu-Ola–Ulugoi Fe–Cu–Au–polymetallic mineralization zone: I.1, East Tannu-Ola Fe–Cu–Au–polymetallic ore district; I.1.1, Elegest–Mezhegei gold ore/gold placer cluster; I.1.2, predicted Irbitei Au–Ag–polymetallic cluster; I.1.3, predicted Aptara gold ore cluster; I.1.3.1, Despen gold ore field; I.1.4, predicted Shivilig gold ore cluster; I.1.4.1, predicted Ongesh gold ore field; I.1.0.1, predicted Ulug-Sailyg Cu–Mo ore field; I.1.0.2, predicted Ak-Chary Au–Mo–Cu ore field.

nites, tonalites, and leucopagliogranoites composing large irregular-shaped bodies with curved borders and large xenolith blocks (outliers) among the granitoids of the Tannu-Ola complex.

The **Tannu-Ola diorite–granodiorite–plagiogranite complex** is formed by rocks of two phases. The first phase makes up 25–30 vol.% of the complex and comprises hornblende diorites (70 vol.% of the phase) and quartz diorites.

Rocks transformed to hybrid diorite-like varieties, gabbro-diorites, and hornblendites as well as xenoliths of the host rocks are found on the periphery of the massifs. The second phase makes up 70–75 vol.% of the complex and comprises biotite–amphibole plagiogranites (predominant), tonalites (up to 40 vol.% of the phase), and quartz diorites.

The rocks of the Tannu-Ola complex form large massifs within the Eastern Tannu-Ola Range and a number of smaller satellites. The massif rock outcrops are of irregular shape, oddly rugged, and vary significantly in size. The area of the smallest body in the Duvelig–Kholu interfluvium is no more than 0.28 km<sup>2</sup>, and the area of the largest (Eastern Tannu-Ola) body reaches 700 km<sup>2</sup>. The massifs are characterized by a minor erosional truncation, which is due to the wide spread of xenoliths of the host rocks, large roof sags, and wide aureoles of exocontact hornfelses and skarns.

**The Argolik granite–leucogranite complex** is formed by binary, two-feldspathic, and alaskite granites, fine-grained leucocratic granites, and granite porphyry. Usually they compose narrow ( $\leq 120$  m) elongate stock-like bodies of irregular shape with vertical or near-vertical contacts, locally accompanied by eruptive breccias. The massifs are often confined to coeval tectonic zones composed of granitoids with prototectonic gneissosity subjected to shearing, foliation, silicification, and epidotization. The granites are often more intensely altered than the host rocks. These stock-like bodies might be tongues of larger massifs that were not denuded by erosion. All massifs have homogeneous composition and structure.

## PETROGRAPHY

Plagiogranites of the second phase are predominant in the Maina-type complex. They are light gray to yellowish-gray and have porphyritic texture and, often, gneissoid structure. The rocks contain plagioclase (40–55%), quartz (40–45%), and biotite (1–3%) and are enriched in green hornblende (10–15%), which is often surrounded by clusters of fine-scaled biotite and accessory minerals. The porphyritic texture of the plagiogranites is due to coarser plagioclase, green hornblende, and quartz grains present in an aggregate of finer grains of the same minerals (Fig. 3). There are also graphic intergrowths of plagioclase and quartz. The rocks of the first phase (hornblende gabbro and quartz-containing gabbro) are composed of plagioclase (50–60%) and green hornblende with clinopyroxene relics in the grain cores (40–50%). Quartz amounts to 1–5%. The zones of transition from gabbroids of the first phase to plagiogranites of the second phase often contain diorites and quartz diorites, which do not form separate bodies with clear borders and might be hybrid rocks. These gray to greenish-gray massive medium-grained rocks are composed of plagioclase (40–55%), K-feldspar (1–3%), quartz (0 to 5–15%), and green hornblende (20–35%). Accessory minerals of the rocks are

apatite, magnetite, and zircon. Secondary minerals are sericitic, light green chlorite, and saussurite, which are developed after plagioclase; hornblende is partly replaced by chlorite, biotite, epidote, and actinolite.

The predominant rocks of the first phase of the Tannu-Ola complex are diorites. These are gray to greenish-gray fine-to medium-grained massive rocks with a subhedral to distinct prismatic texture. They have a varying amount of dark-colored minerals, often contain numerous xenoliths of the host rocks, and grade into gabbro and quartz diorites. Major minerals are plagioclase (40–65%) and brown to greenish-brown hornblende (20–35%).

The rocks of the second phase of the Tannu-Ola complex are often a continuous series from tonalites to plagiogranites, with variation in the quantitative proportion of rock-forming minerals. The rock varieties grade into each other. For example, in the range 0–50 m in the lower stream of the Kholu River, quartz diorites are gradually changed by tonalites and granodiorites and then by plagiogranites. They preserve structures and textures; only the contents and proportions of rock-forming minerals change.

The rocks are gray to pinkish-gray medium- and coarse-grained, with a subhedral texture. They are composed of plagioclase (40–65%), quartz (25–45%), and biotite (up to 5%) and lack primary K-feldspar. The rocks of the plagiogranite–tonalite transition and peripheral (endocontact) zones contain brownish-green hornblende (0–10%). Plagiogranites of the fault and fractured zones are subjected to K-feldspathization leading to the reactionary replacement of plagioclase by microcline. In places, plagioclase has been preserved only as fragments in K-feldspar grains. Other secondary alterations of the rocks are sericitization, epidotization, and chloritization. Biotite often replaces hornblende. Major accessory minerals of the Tannu-Ola complex rocks are sphene, apatite, magnetite, zircon, and pyrite.

Biotite granites are the main rocks of the Argolik complex. These are red to meat-red medium-grained, often porphyritic, rocks with a granophytic texture. They are composed of albite (5–10%), K-feldspar (50–65%), quartz (30–50%), and biotite (1–5%). The porphyritic texture is due to the present coarser orthoclase grains. Biotite is almost completely replaced by chlorite. Secondary minerals are epidote, chlorite, and leucoxene. The Argolik granites contain a wide spectrum of accessory minerals: zircon, monazite, orthite, sphene, apatite, and fluorite.

## PETROCHEMISTRY AND GEOCHEMISTRY

The rocks from gabbro to plagiogranites of the Maina-type complex form a single evolutionary trend corresponding to a high-Na low-alkali rock series (Fig. 4a). In the CaO–Sr diagram, the configurative points of these rocks form a tholeiite trend (Fig. 4h) indicating their genetic belonging to a gabbro–granitoid association. As the SiO<sub>2</sub> con-

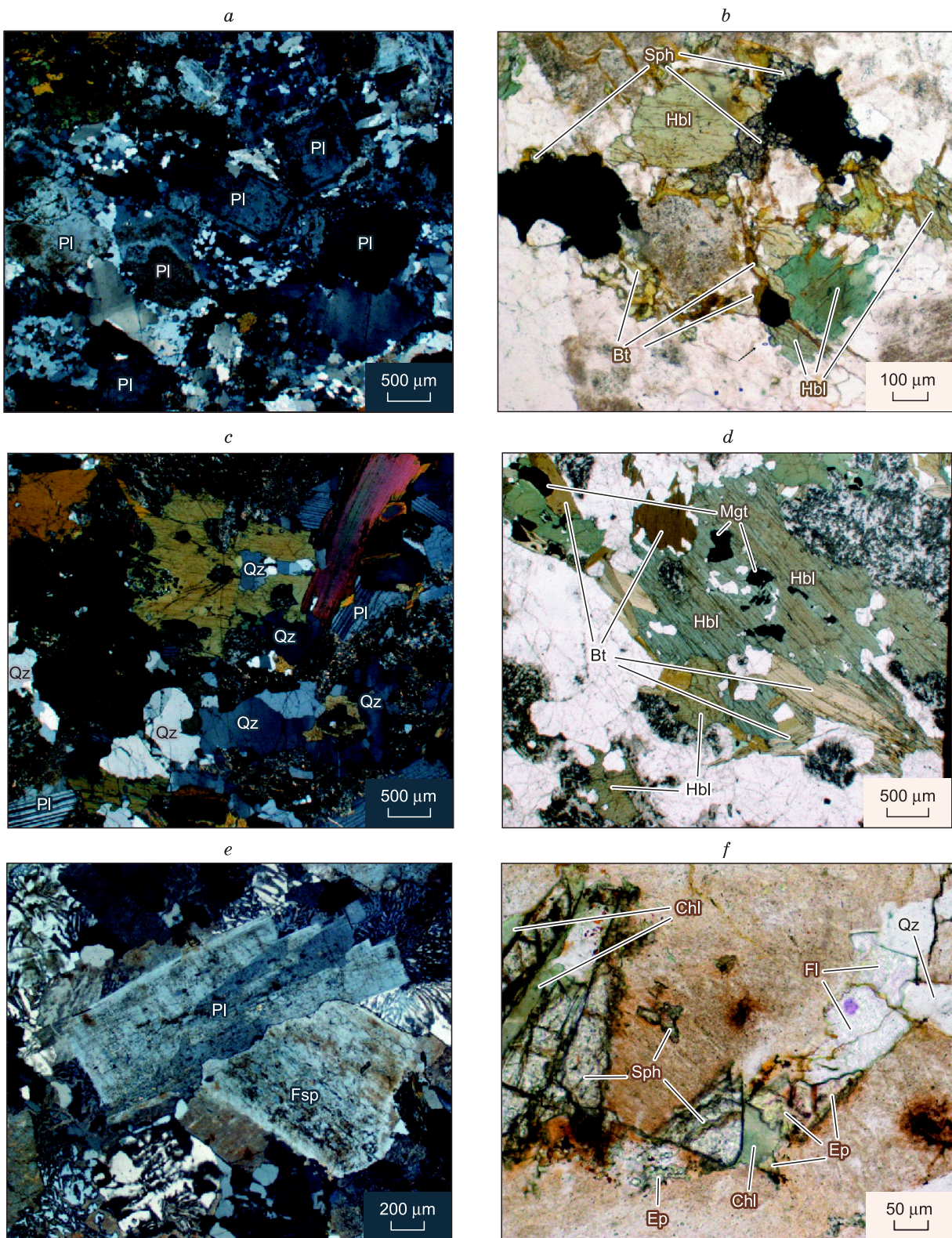


**Fig. 3.** Structures and textures of the granitoids of the Maina-type (*a*, *b*), Tannu-Ola (*c*, *d*), and Argolik (*e*, *f*) complexes of the Ungesh pluton. *a*, *b*, Hornblende-biotite plagiogranite (slice 2135-1); *c*, *d*, biotite-hornblende quartz diorite (slice 77); *e*, *f*, biotite leucogranite (slice 2226-1). *a*, *c*, *e*,  $\times$ Nicol photomicrograph; *b*, *d*, *f*, transmission photomicrograph. Pl, plagioclase; Fsp, K-feldspar; Qz, quartz; Hbl, hornblende; Bt, biotite; Chl, chlorite; Ep, epidote; Sph, sphene; Fl, fluorite; Mgt, magnetite.

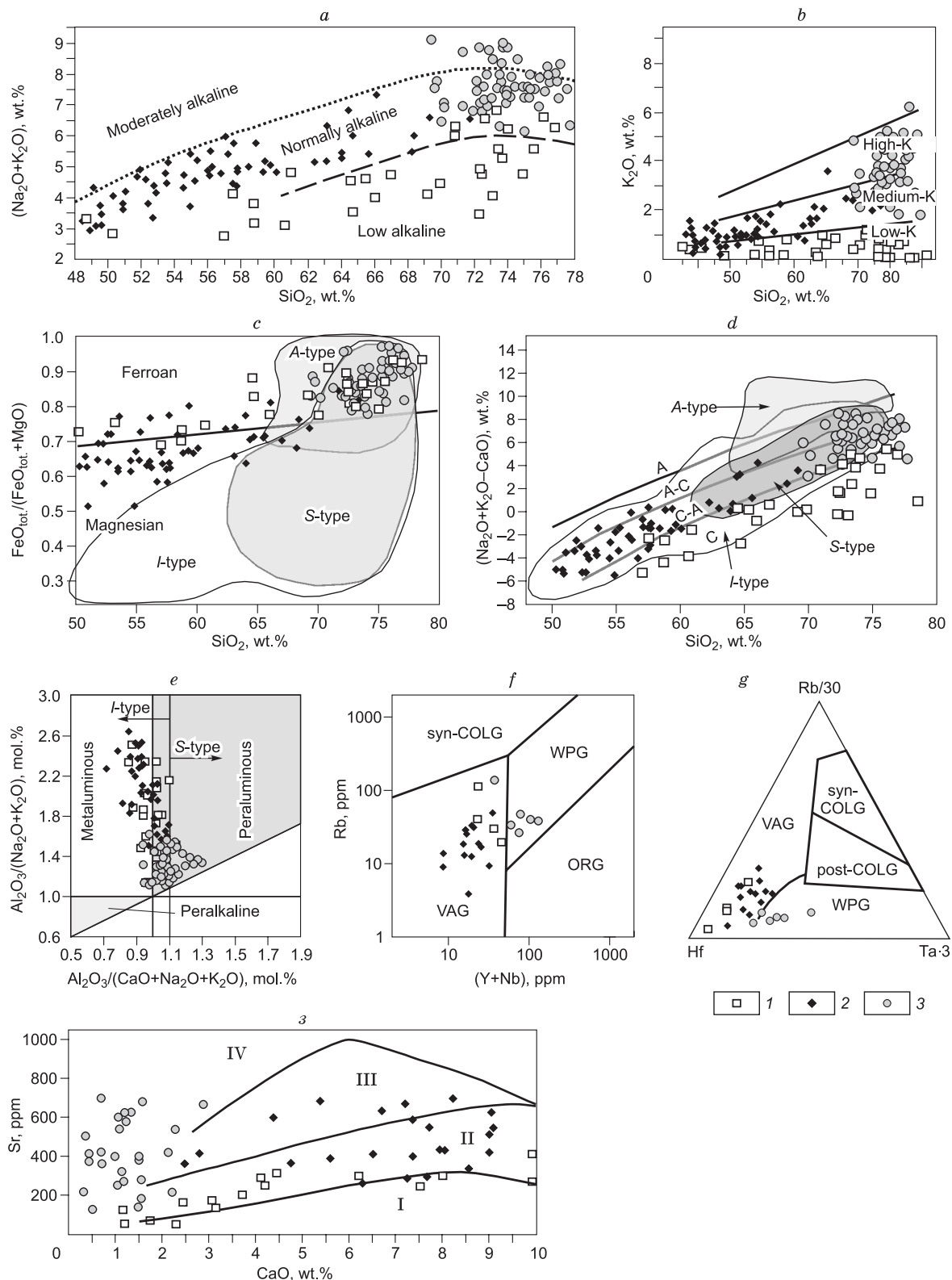


**Fig. 4.** Classification and discrimination diagrams for the granitoids of the Maina-type (1), Tannu-Ola (2), and Argolik (3) complexes. *a*, TAS diagram; *b*,  $K_2O$ - $SiO_2$  diagram; *c-e*, Frost diagrams (Frost et al., 2001) ( $c-f = FeO_{tot}/(FeO_{tot} + MgO)$ ); *d*, MALI; *e*, ASI; *f*, Pearce discrimination diagram (Pearce et al., 1984); *g*, Harris ternary diagram (Harris et al., 1986); *h*,  $CaO$ - $Sr$  diagram. Rock series: C, calcic, C-A, calc-alkalic, A-C, alkali-calcic, A, alkalic. Fields of: syn-COLG, syncollisional granites, post-COLG, postcollisional granites, WPG, within-plate granites, VAG, volcanic-arc granites, ORG, oceanic-ridge granites. Fields of magma-derived rocks (Fershtater et al., 1984): I, oceanic tholeiitic, II, continental and island-arc tholeiitic, III, high-alkali tholeiitic and andesitic, IV, latictic, high-alkali tholeiitic, and alkali-basaltic. The boundaries of the fields of rocks of different alkalinity are given after Bogatikov et al. (2009).

Table 1. Average contents of major, rare-earth, and trace elements

Com- ponent	1	2	3	4	5	6	7	8	9	10	11	12
SiO <sub>2</sub>	50.08±2.21	57–61 58.93±1.61	64.6–67 65.58±0.97	69.2–72.6 71.55±1.36	73.1–78.6 74.98±1.64	48.4–52.8 51.04±1.47	53.4–56.7 55.04±1.08	57.1–63.1 59.05±2.06	64–66.1 65.2±0.87	68.2–71 70.22±1.85	69.4–72.8 71.69±1.25	73–77.7 75.1±1.36
Al <sub>2</sub> O <sub>3</sub>	15.6–17.3 16.4±0.83	15.11–17.7 16.49±1.02	13.8–16 14.92±0.8	11.5–14.6 13.21±0.97	10.3–14.3 12.59±1.1	15.9–19.5 17.59±1.03	16.57–18.9 17.81±0.8	14.2–18.2 16.97±1.42	14.9–17 15.53±0.94	14.8–15.7 15.25±0.34	12.72–15.3 13.78±0.76	10.2–14.19 12.73±0.73
TiO <sub>2</sub>	0.86–1.26 1.02±0.19	0.4–0.8 0.66±0.15	0.38–0.9 0.54±0.21	0.3–0.5 0.41±0.07	0.16–0.42 0.27±0.11	0.33–1.61 0.9±0.27	0.7–1.63 0.84±0.25	0.22–1.9 0.56±0.1	0.44–0.74 0.3±0.13	0.17–0.46 0.34±0.08	0.2–0.52 0.21±0.08	0.01–0.33 0.21±0.08
$\Sigma \text{Fe}_2\text{O}_3$	9.3–13.8 12.1±2.01	5.8–9 7.67±1.17	4.5–9.3 6.3±1.98	3.1–6.6 4.41±1.21	1.4–4.3 2.57±0.69	7–11.5 9.27±1.3	6.3–10.4 7.4±1.01	5.5–9.7 6.65±1.54	3.7–5.4 4.68±0.6	2–4 2.94±0.96	2–4.2 2.97±0.58	1–3.5 2.1±0.57
MnO	0.17–0.24 0.2±0.03	0.08–0.14 0.12±0.03	0.1–0.22 0.13±0.05	0.05–0.14 0.09±0.03	0.02–0.07 0.04±0.02	0.12–0.27 0.15±0.04	0.1–0.36 0.12±0.07	0.03–0.17 0.11±0.03	0.06–0.1 0.09±0.01	0.04–0.07 0.06±0.01	0.02–0.13 0.05±0.02	0.01–0.07 0.04±0.02
MgO	4.3–7.2 5.5±1.33	2.6–5.8 3.68±1.2	1.3–2.1 1.68±0.32	0.3–1.4 0.8±0.33	9.3–13.8 0.44±0.24	3.4–9.5 5.52±1.73	2.6–4.9 4.29±0.93	2.1–4.2 3.2±0.91	1.1–2.9 1.73±0.63	0.34–1.9 0.98±0.58	0.2–1.1 0.55±0.21	0.1–0.7 0.26±0.14
CaO	4.6–10.3 8.68±2.72	6.3–8.1 6.9±0.71	4.1–6.2 4.76±0.85	1.6–4.2 3.05±0.92	0.8–4.4 2.03±1.06	7.4–12.5 9.12±1.5	5.6–9.3 7.68±0.99	4.4–7.7 6.17±0.9	2.8–5.3 3.45±0.98	2.51–4.1 3.08±0.61	0.3–3.4 1.41±0.76	0.1–1.8 0.96±0.54
Na <sub>2</sub> O	2.3–5.2 3.28±1.31	2.6–4 3.25±0.49	3.4–4.3 3.74±0.36	3.4–4.9 4.03±0.48	3.3–6.6 4.82±1.17	1.1–3.5 3.04±0.73	2.9–4.8 3.68±0.54	2.57–4.6 3.92±0.69	3.4–4.4 4.08±0.48	3.5–5.1 4.28±0.55	2.9–5.1 3.98±0.59	2–4.64 3.67±0.81
K <sub>2</sub> O	0.1–0.6 0.4±0.22	0.2–0.8 0.42±0.3	0.1–0.9 0.58±0.35	0.1–1.1 0.6±0.36	0.1–0.8 0.38±0.32	0.2–1.54 0.71±0.43	0.5–1.1 0.99±0.25	0.9–2.25 1.25±0.37	1.4–3.6 2.35±0.79	1.2–2.5 1.99±0.5	2.1–4.9 3.56±0.9	2.7–6.2 3.99±0.94
P <sub>2</sub> O <sub>5</sub>	0.06–0.25 0.13±0.09	0.03–0.17 0.11±0.05	0.08–0.3 0.14±0.09	0.07–0.1 0.08±0.03	0.03–0.1 0.04±0.03	0.04–0.31 0.18±0.08	0.1–0.54 0.18±0.12	0.08–0.41 0.2±0.08	0.1–0.21 0.15±0.05	0.05–0.1 0.09±0.03	0.01–0.11 0.07±0.03	0.01–0.08 0.33±0.03
LOI	0.8–2.9 1.75±0.91	0.6–2.38 1.36±0.71	0.83–1.44 1.25±0.25	0.21–3.01 1.03±0.86	0.36–1.8 0.72±0.4	0.08–3 1.96±0.74	0.78–2.16 1.41±0.44	0.8–2.41 1.49±0.56	0.8–1.66 1.07±0.32	0.35–1.4 0.76±0.44	0.3–1.9 0.94±0.39	0.12–3.41 0.65±0.47
Total	98.98–100.46 99.53±0.64	98.72–100.22 99.59±0.65	98.66–100.66 99.63±0.83	98.5–101.35 99.76±0.98	98.83–100.69 99.55±0.56	98.44–100.63 99.47±0.72	99.08–100.46 99.61±0.63	98.49–100.37 99.74±0.62	98.82–100.33 99.33±0.58	99.33–100.39 99.93±0.38	98.41–100.35 99.33±0.63	98.55–102.08 99.72±0.78
La	4.42	—	7.51	15.13	9.78	7.11	7.6	9.3	—	11.69	—	28.74
Ce	11.7	—	16.4	34.4	20.06	16.44	17.77	20.33	—	26.35	—	79.87
Pr	1.85	—	2.51	4.71	2.57	2.48	2.65	2.76	—	3.32	—	8.91

(continued on next page)

**Table 1 (continued)**

Com- ponent	1	2	3	4	5	6	7	8	9	10	11	12
Nd	9.06	—	11.4	20.37	11.3	12.48	13.56	12.52	—	13.2	—	38.9
Sm	2.75	—	2.92	5.06	3	3.28	3.35	3.08	—	2.91	—	9.92
Eu	0.91	—	0.72	0.94	0.82	1.07	1.35	0.87	—	0.73	—	1.27
Gd	2.88	—	2.57	4.46	2.98	2.93	3.14	2.78	—	2.46	—	8.95
Tb	0.51	—	0.46	0.81	0.61	0.51	0.52	0.44	—	0.42	—	1.74
Dy	3.44	—	2.92	5.37	4.29	3.05	3.15	2.96	—	2.71	—	13.2
Ho	0.73	—	0.6	1.2	1.01	0.63	0.63	0.64	—	0.58	—	3.02
Er	1.95	—	1.74	3.39	2.83	1.62	1.65	1.61	—	1.61	—	8.4
Tm	0.27	—	0.29	0.56	0.45	0.23	0.23	0.24	—	0.25	—	1.21
Yb	1.97	—	1.86	4.07	3.41	1.62	1.53	1.62	—	1.76	—	8.41
Lu	0.31	—	0.31	0.68	0.46	0.24	0.23	0.25	—	0.25	—	1.28
Rb	7.88	—	11.7	34.37	38.34	17.33	8.54	19.33	—	32.85	—	36.76
Sr	322	—	313	114.7	108.1	407.5	531.3	443.75	—	323.3	—	29.04
Y	19.49	—	18.1	32.63	26.25	17.15	14.36	16.04	—	16.13	—	73.16
Zr	52.1	—	107	217	96.63	72.2	68.73	81.85	—	129.6	—	274.9
Nb	1.2	—	1.28	6.57	2.93	1.6	2.06	3.29	—	5.64	—	19.83
Cs	0.23	—	0.31	0.31	0.28	0.32	0.22	0.3	—	0.51	—	0.3
Ba	267.45	—	389	533.8	313.7	312.8	281	358.75	—	632.8	—	506.2
Hf	1.1	—	2.89	6.11	3.02	1.91	1.88	2.19	—	3.53	—	8.71
Ta	0.12	—	0.11	0.45	0.28	0.12	0.14	0.22	—	0.46	—	1.34
Th	0.45	—	2.12	6	3.45	0.71	0.97	1.83	—	3.49	—	5.51
U	0.2	—	0.92	0.98	0.6	0.35	0.44	0.48	—	0.83	—	1.44
Pb	3.34	—	4.63	2.68	7.27	4.35	3.87	6.41	—	6.63	—	4.89

Note. Maina-type complex: 1, gabbro (4/4); 2, quartz diorites (6); 3, granodiorites (5/1); 4, plagiogranites (8/3); 5, leucophaeites (12/3); Tannu-Ola complex: 6, gabbro (19/4); 7, diorites (14/3); 8, quartz diorites (16/4); 9, granodiorites (6); 10, plagiogranites (6/4); Argolik complex: 11, granites (20); 12, leucogranites (48/9). Parenthesized is the number of analyses used for the calculation of the average contents of major (wt.%) and rare-earth and trace (ppm) elements. The values above the line are the element limits, and those below the line are the average contents  $\pm$  root-mean-square deviations.

tent increases, the  $\text{Na}_2\text{O} + \text{K}_2\text{O}$  also increases and the  $\text{Al}_2\text{O}_3$ ,  $\text{CaO}$ ,  $\text{MgO}$ ,  $\text{MnO}$ ,  $\Sigma\text{Fe}_2\text{O}_3$ , and  $\text{TiO}_2$  contents decrease. These are ferroan ( $f = \text{FeO}_{\text{tot}}/(\text{FeO}_{\text{tot}} + \text{MgO}) = 0.6\text{--}0.9$ ) calcic granitoids (Fig. 4c, d; Table 1).

The granitoids of the Maina-type complex are characterized by low contents of Rb (2–60 ppm) and Nb (0–4 ppm), medium contents of Sr (160–300 ppm) and Zr (100–260 ppm), and a wide range of contents of Ba (100–800 ppm), Y (10–60 ppm), Ce (3–40 ppm), and Yb (1–4 ppm). Their chondrite-normalized REE patterns show domination of LREE over HREE and a negative Eu anomaly ( $(\text{La/Yb})_N = 1.5\text{--}6.0$ ;  $(\text{Eu/Eu}^*)_N = 0.5\text{--}0.8$ ). The multielement patterns of the Maina-type plagiogranites show positive Pb and negative Ta and Nb anomalies, P and Ti minima, and a slight Sr maximum (Fig. 5). In the discrimination diagrams, the figurative points of the Maina-type plagiogranites fall in the fields of island-arc granitoids (Fig. 4f, g).

The rocks of the Tannu-Ola complex are characterized by a wide range of  $\text{SiO}_2$  (48–72 wt.%) and total alkali (3.0–7.5%) contents, domination of Na over K, and high contents of Ca (3–10%). Most of the Tannu-Ola granitoids are normal and alkaline (mostly sodium) (Fig. 4a) magnesian ( $f = 0.5\text{--}0.8$ ) rocks of calcic and calc-alkalic series (Fig. 4c, d).

The Tannu-Ola granitoids have low contents of Rb (2–30 ppm), Zr (50–120 ppm), Nb (1–7 ppm), Y (10–30 ppm), Ce (10–30 ppm), and Yb (1–3 ppm), a wide range of Ba contents (50–600 ppm), and high contents of Sr (200–700 ppm). Their chondrite-normalized REE patterns show a low total REE content, domination of LREE over HREE, and no negative Eu anomaly ( $(\text{La/Yb})_N = 2\text{--}9$ ;  $(\text{Eu/Eu}^*)_N = 0.7\text{--}2.0$ ). The multielement patterns of these rocks show positive Sr and Pb and negative Ta and Nb anomalies and P and Ti minima (Fig. 5). The discrimination diagrams (Fig. 4f, g) demonstrate a compositional similarity of the Tannu-Ola rocks to island-arc granitoids.

According to petrogeochemical composition, the Argolik granitoids are calc-alkalic potassic rocks. The  $\text{K}_2\text{O} + \text{Na}_2\text{O}$  content (6.5–8.5 wt.%) regularly increases in the granite-leucogranite series (Fig. 4a), primarily because of the increase in  $\text{K}_2\text{O}$  content (2–5 wt.%). The content of  $\text{Na}_2\text{O}$  varies insignificantly and decreases from 5 to 2.5 wt.% as the content of  $\text{SiO}_2$  increases. The Argolik granitoids are ferroan ( $f = 0.8\text{--}1.0$ ) alkali-calcic and calc-alkalic rocks (Fig. 4c, d).

The Argolik granitoids have medium contents of Rb (25–130 ppm), Sr (15–140 ppm), and Zr (130–350 ppm), widely varying contents of Ba (50–980 ppm), Nb (10–30 ppm), Y (10–100 ppm), and Ce (30–140 ppm), and high contents of Yb (4–14 ppm). Their chondrite-normalized REE patterns (Fig. 5) show domination of LREE over HREE and a negative Eu anomaly ( $(\text{La/Yb})_N = 2.5\text{--}7.0$ ;  $(\text{Eu/Eu}^*)_N = 0.4\text{--}0.5$ ). The multielement patterns of these rocks show positive Pb and weak negative Ta and Nb anomalies, HFSE enrichment, and distinct Sr, P, and Ti minima (Fig. 5). The discrimination diagrams (Fig. 4f, g) demonstrate a similarity of the Argolik leucogranites to within-plate granitoids.

## RESULTS OF GEOCHRONOLOGICAL (U/Pb) AND ISOTOPE-GEOCHEMICAL (Rb-Sr, Sm-Nd) STUDIES

Geochronological U/Pb (SHRIMP II) studies of zircons from the Ungesh pluton granitoids yield the following time intervals of formation of the above rock complexes: Maina-type,  $534 \pm 3$  to  $518 \pm 3$  Ma; Tannu-Ola,  $507.8 \pm 6.4$  to  $469.2 \pm 5.5$  Ma; and Argolik,  $451 \pm 4$  to  $447 \pm 2$  Ma (Fig. 6, Tables 2 and 3).

The U/Pb isotope studies were carried out for zircons from bulk samples of major rocks from the Ungesh pluton (Fig. 6, Tables 2 and 3). We studied hornblende gabbro

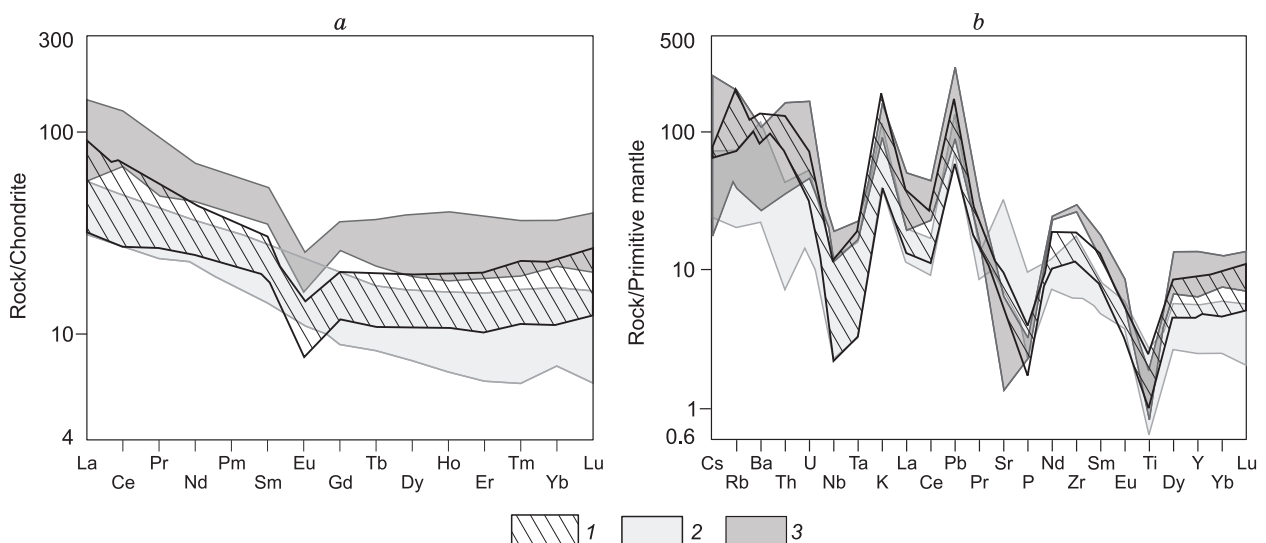


**Fig. 5.** Chondrite-normalized (Sun and McDonough, 1989) REE (a) and multielement (b) patterns of the rocks of the Maina-type (1), Tannu-Ola (2), and Argolik (3) complexes.

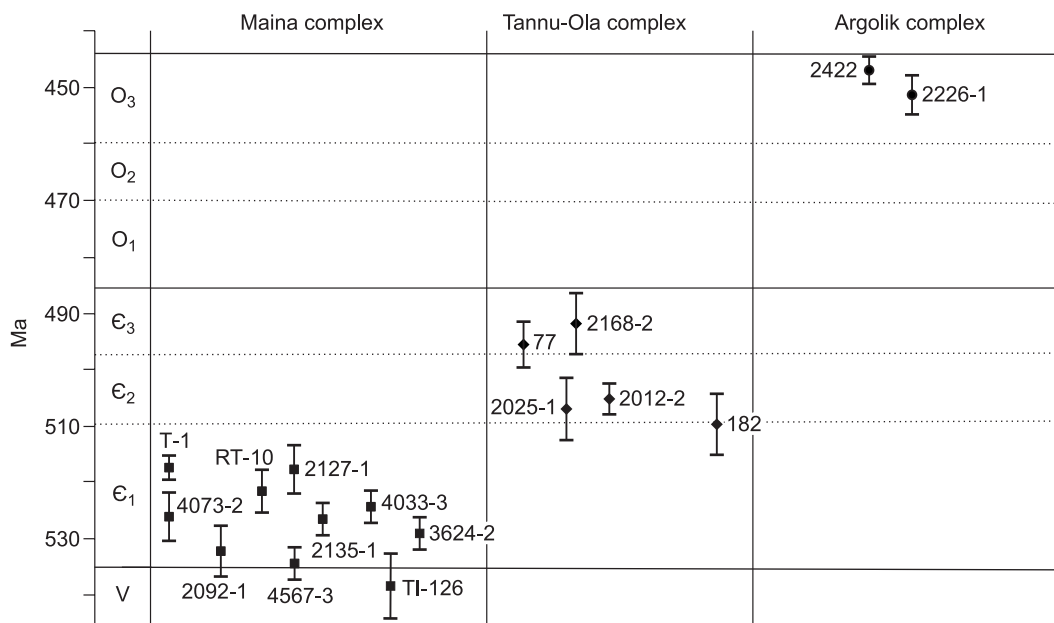


**Fig. 6.** Results of U/Pb isotope dating of the granitoids of the Ungesh pluton. Sample 182, data after Gusev et al. (2014); samples TI-126 and T-1, after Mongush et al. (2011); and sample RT-10, after Rudnev et al. (2006).

(sample 3624-2) of the first phase and biotite (hornblende-biotite) plagiogranites of the second phase (samples 4567-3, 2092-1, 2135-1, 4073-2, 4033-3, and 2127-1) from the Maina-type complex. Zircons from these rocks are yellow and pinkish-yellow transparent to semitransparent euhedral prismatic crystals 120–260  $\mu\text{m}$  in average length, with cracks and reddish-brown inclusions; their average elongation index is 1.3–2.6. In cathodoluminescence (CL) images, the zircons are moderately or brightly luminescent and have a thick or, less often, thin sector zoning (Fig. 7a, b).

The concordant age was estimated from 8–10 measurements for all zircons from the rocks of the Maina-type complex; the concordance probability varies from 0.046 to 0.9 (Fig. 8). Taking into account the morphology of zircons, we relate the formation of these rocks to the early Cambrian (534–518 Ma) magmatic events.

The Sm/Nd and Rb/Sr isotope studies were performed for plagiogranite of the Maina-type complex (sample 2092-1). The results (Table 4) show a high primary  $^{143}\text{Nd}/^{144}\text{Nd}$  value ( $\epsilon_{\text{Nd}}(T) = 5.02$ ) and a low primary  $^{87}\text{Sr}/^{86}\text{Sr}$  value (0.704216).

**Table 2.** Results of U/Pb dating (SHRIMP-II) of intrusive rocks from the Ungesh pluton

Complex	Sample	Number of measurements	Rock. Massif. Phase	Age, Ma
Maina-type	3624-2	10	Hornblende gabbro. Irbitei massif. First phase	$529 \pm 3$
	4567-3	8	Porphyritic plagiogranite. Dyttyg-Khem massif. Second phase	$534 \pm 3$
	2092-1	10	Hornblende plagiogranite. Biche-Sailyg massif. Second phase	$532.2 \pm 5.2$
	2135-1	10	Hornblende–biotite plagiogranite. Western part of Nizhnii Irbitei massif. Second phase	$527 \pm 3$
	4073-2	10	Porphyritic plagiogranite. Aptara massif. Second phase	$526 \pm 4$
	4033-3	10	Hornblende–biotite plagiogranite. Central part of Nizhnii Irbitei massif. Second phase	$524 \pm 3$
	2127-1	9	Biotite plagiogranite. Periphery of Nizhnii Irbitei massif. Second phase	$518 \pm 3$
Tannu-Ola	2168-2	10	Hornblende diorite. Central part of East Tannu-Ola massif. First phase	$492.2 \pm 5.5$
	77	10	Hornblende diorite. Periphery of Tei-Dash massif. First phase	$496 \pm 4.9$
	2012-2	10	Porphyritic plagiogranite. Khovu-Aksy massif. Second phase	$505 \pm 3$
	2025-1	10	Porphyritic plagiogranite. Ust'-Ungesh massif. Second phase	$507.8 \pm 6.4$
Argolik	2226-1	10	Biotite leucogranite. Kyzyl-Dag massif	$451 \pm 4$
	2422	10	Biotite–hornblende leucogranite. Biche-Serlig massif	$447 \pm 2$

**Table 3.** Results of U/Pb isotope studies (SHRIMP-II) of single zircon grains from the Ungesh pluton rocks

Sample, point	$^{206}\text{Pb}_{\text{e}}$ , %	U ppm	T ppm	$^{232}\text{Th}/^{238}\text{U}$	$^{206}\text{Pb}^*$ , ppm	$^{206}\text{Pb}/^{238}\text{U}$	$^{207}\text{Pb}/^{206}\text{Pb}$	Isotopic age	$^{238}\text{U}/^{206}\text{Pb}$ discordance, %	Error, $^{207}\text{Pb}/^{235}\text{U}$ $\pm \%$	Error, $^{206}\text{Pb}^*/^{238}\text{U}$ $\pm \%$	Error, $^{207}\text{Pb}^*/^{238}\text{U}$ $\pm \%$	Correlation coefficient
Maina-type gabbro-plagiogranite complex													
Hornblende gabbro													
3624-2_1.1	0.77	115	69	0.62	8.62	534.2	$\pm 6.2$	283	$\pm 180$	-47	11.57	1.2	0.619
3624-2_2.1	2.73	243	149	0.63	18.5	532.2	$\pm 5.2$	388	$\pm 220$	-27	11.61	1	0.646
3624-2_3.1	0.19	210	141	0.70	15.4	528.3	$\pm 4.4$	498	$\pm 66$	-6	11.71	0.87	0.0572
3624-2_4.1	0.64	174	72	0.43	13	534.7	$\pm 5.1$	575	$\pm 130$	8	11.56	1	0.0592
3624-2_5.1	0.00	87	45	0.54	6.38	529.8	$\pm 6.7$	605	$\pm 79$	14	11.67	1.3	0.0601
3624-2_6.1	0.01	198	99	0.52	14.5	526.3	$\pm 4.5$	552	$\pm 58$	5	11.76	0.89	0.0586
3624-2_7.1	0.70	177	118	0.69	13.1	530.2	$\pm 5.2$	251	$\pm 160$	-53	11.66	1	0.0512
3624-2_8.1	1.21	137	84	0.64	10.1	523	$\pm 6.2$	211	$\pm 240$	-60	11.83	1.2	0.0503
3624-2_9.1	0.00	143	86	0.62	10.5	528.4	$\pm 5.3$	540	$\pm 68$	2	11.71	1	0.0583
3624-2_10.1	0.26	220	135	0.63	16	522.6	$\pm 5.1$	569	$\pm 87$	9	11.84	1	0.0591
Porphyritic plagiogranite													
4567-3_8.1	0.14	508	257	0.52	33.4	475	$\pm 8.1$	596	$\pm 45$	26	13.080	1.8	0.0598
4567-3_10.1	0.10	461	264	0.59	32.6	509	$\pm 3.2$	539	$\pm 42$	6	12.167	0.7	0.0583
4567-3_7.1	0.24	343	219	0.66	25.2	529	$\pm 3.7$	509	$\pm 62$	-4	11.703	0.7	0.0574
4567-3_4.1	0.28	205	138	0.70	15.1	530	$\pm 4.5$	511	$\pm 78$	-4	11.67	0.9	0.0575
4567-3_3.1	0.23	838	726	0.89	61.9	530	$\pm 2.5$	620	$\pm 39$	17	11.663	0.5	0.0605
4567-3_2.1	0.00	223	86	0.40	16.5	532	$\pm 4.2$	561	$\pm 49$	5	11.619	0.8	0.0588
4567-3_9.1	0.07	739	497	0.70	54.9	535	$\pm 3.1$	513	$\pm 32$	-4	11.557	0.6	0.05756
4567-3_5.1	0.18	340	122	0.37	25.4	536	$\pm 4.1$	519	$\pm 54$	-3	11.538	0.8	0.0577
4567-3_1.1	0.00	410	275	0.69	30.6	538	$\pm 3.3$	532	$\pm 37$	-1	11.498	0.6	0.05805
4567-3_6.1	1.16	238	141	0.61	18	539	$\pm 5.1$	696	$\pm 160$	29	11.46	1	0.0626
Hornblende plagiogranite													
2092-1_1.1	0.51	174	32	0.19	13	534.7	$\pm 7.4$	536.3	$\pm 7.4$	-16	11.5	1.4	0.0601
2092-1_2.1	0.28	107	17	0.16	7.87	527.3	$\pm 7.9$	527.6	$\pm 8.1$	-3	11.7	1.6	0.0598
2092-1_3.1	0.25	118	17	0.15	8.79	532.7	$\pm 8$	532.3	$\pm 8.2$	5	11.58	1.6	0.0608
2092-1_4.1	0.00	101	10	0.10	7.48	531.9	$\pm 8.2$	533.4	$\pm 8.4$	-17	11.63	1.6	0.0557
2092-1_5.1	0.56	87	10	0.11	6.48	533.9	$\pm 9$	536	$\pm 8.8$	-23	11.51	1.7	0.0596
2092-1_6.1	0.00	111	17	0.16	8.33	539.5	$\pm 8$	539.3	$\pm 8.2$	2	11.46	1.6	0.0585
2092-1_7.1	0.34	87	10	0.12	6.3	519.3	$\pm 9.1$	520.1	$\pm 9.5$	-9	11.88	1.8	0.0592
2092-1_8.1	0.58	112	20	0.19	8.57	545.9	$\pm 8.2$	547.3	$\pm 8.3$	-14	11.25	1.5	0.0612
2092-1_9.1	0.42	94	12	0.13	6.91	527.4	$\pm 8.2$	528.6	$\pm 8.3$	-12	11.68	1.6	0.0597
2092-1_10.1	0.00	112	18	0.17	8.27	530.9	$\pm 7.7$	529.6	$\pm 7.9$	14	11.65	1.5	0.06

(continued on next page)

Table 3 (continued)

Sample, point	$^{206}\text{Pb}_e$ , ppm	$\frac{\text{U}}{\text{ppm}}$	$\frac{\text{T}}{\text{ppm}}$	$^{232}\text{Th}/^{238}\text{U}$	$^{206}\text{Pb}^*$ , ppm	$^{206}\text{Pb}/^{238}\text{U}$	$^{207}\text{Pb}/^{206}\text{Pb}$	Error, $\pm\%$	$^{238}\text{U}/^{206}\text{Pb}$	Error, $\pm\%$	$^{207}\text{Pb}^*/^{235}\text{U}$	Error, $\pm\%$	$^{208}\text{Pb}^*/^{238}\text{U}$	Error, $\pm\%$	Correlation coefficient				
<b>Hornblende plagiogranite</b>																			
2135-1_1.1	0.14	421	323	0.79	31.1	531.8	$\pm 3.4$	525	$\pm 63$	-1	11.627	0.67	0.0579	0.67	0.686	2.9	0.086	3	0.23
2135-1_2.1	0.00	180	80	0.46	13	521.3	$\pm 4.8$	507	$\pm 63$	-3	11.87	0.96	0.0574	0.96	0.667	2.8	0.0822	3	0.32
2135-1_3.1	0.57	223	96	0.44	16.4	528.7	$\pm 4.8$	382	$\pm 130$	-28	11.7	0.94	0.0543	0.94	0.64	5.7	0.08547	5.8	0.16
2135-1_4.1	0.00	151	79	0.54	11.1	528.3	$\pm 6.1$	502	$\pm 68$	-5	11.71	1.2	0.0573	1.2	0.674	3.1	0.0854	3.3	0.36
2135-1_5.1	0.37	257	154	0.62	19	530.9	$\pm 4.5$	450	$\pm 110$	-15	11.65	0.89	0.0559	0.89	0.662	4.8	0.08584	4.9	0.18
2135-1_6.1	0.00	99	34	0.36	7.23	527.6	$\pm 6.7$	632	$\pm 80$	20	11.72	1.3	0.0608	1.3	0.715	3.7	0.0853	4	0.33
2135-1_7.1	1.21	133	56	0.44	9.64	516.8	$\pm 6.3$	256	$\pm 220$	-51	11.98	1.3	0.0513	1.3	0.591	9.4	0.0835	9.5	0.13
2135-1_8.1	0.74	210	113	0.55	15.6	529.5	$\pm 5.1$	290	$\pm 150$	-45	11.68	1	0.0521	1	0.615	6.5	0.08561	6.6	0.15
2135-1_9.1	0.40	222	125	0.58	16.1	519.8	$\pm 4.7$	457	$\pm 97$	-12	11.91	0.94	0.0561	0.94	0.65	4.4	0.08397	4.5	0.21
2135-1_10.1	0.35	307	194	0.65	22.4	523.8	$\pm 5$	502	$\pm 120$	-4	11.81	0.99	0.0573	0.99	0.668	5.4	0.08465	5.5	0.18
<b>Porphyritic plagiogranite</b>																			
4073-2.1.1	0.20	260	90	0.36	18.9	522	4.0	496	$\pm 61$	-5	11.849	0.8	0.0571	2.8	0.665	2.9	0.0844	0.8	0.28
4073-2.2.1	0.20	265	82	0.32	19.7	534	4.7	432	$\pm 62$	-19	11.58	0.9	0.0555	2.8	0.661	2.9	0.0864	0.9	0.31
4073-2.3.1	0.21	214	60	0.29	15.7	528	5.1	517	$\pm 65$	-2	11.71	1.0	0.0577	3.0	0.679	3.1	0.0854	1.0	0.32
4073-2.4.1	0.18	353	140	0.41	25.6	521	3.6	589	$\pm 54$	13	11.886	0.7	0.0596	2.5	0.691	2.6	0.0841	0.7	0.28
4073-2.5.1	0.22	299	84	0.29	21.6	520	3.9	473	$\pm 65$	-9	11.908	0.8	0.0565	3.0	0.654	3.1	0.0840	0.8	0.25
4073-2.6.1	0.00	191	43	0.23	14.2	534	4.7	586	$\pm 55$	10	11.58	0.9	0.0595	2.5	0.709	2.7	0.0863	0.9	0.34
4073-2.7.1	0.22	310	99	0.33	22.5	521	3.9	518	$\pm 63$	-1	11.875	0.8	0.0577	2.9	0.67	3.0	0.0842	0.8	0.26
4073-2.8.1	0.00	255	66	0.27	18.5	521	4.1	580	$\pm 49$	11	11.874	0.8	0.0593	2.3	0.689	2.4	0.0842	0.8	0.34
4073-2.9.1	0.32	211	66	0.32	15.7	533	4.8	452	$\pm 87$	-15	11.6	0.9	0.056	3.9	0.665	4.0	0.0862	0.9	0.23
4073-2.9.2	0.17	386	127	0.34	28.8	536	3.6	418	$\pm 56$	-22	11.544	0.7	0.0551	2.5	0.658	2.6	0.0866	0.7	0.27
<b>Hornblende-biotite plagiogranite</b>																			
4033-3_1.1	0.88	215	99	0.48	15.6	517.5	$\pm 5.4$	586	$\pm 110$	13	11.96	1.1	0.0595	4.9	0.686	5	0.0836	1.1	0.22
4033-3_2.1	0.38	155	45	0.30	11.3	525.8	$\pm 5.5$	537	$\pm 150$	2	11.76	1.1	0.0582	7.1	0.682	7.2	0.08499	1.1	0.15
4033-3_3.1	0.60	419	316	0.78	30.5	521.5	$\pm 4$	544	$\pm 90$	4	11.865	0.8	0.0584	4.1	0.678	4.2	0.08426	0.8	0.19
4033-3_4.1	0.89	130	37	0.30	9.62	526.9	$\pm 6$	374	$\pm 150$	-29	11.74	1.2	0.0541	6.7	0.635	6.8	0.0852	1.2	0.18
4033-3_5.1	0.55	136	40	0.30	9.95	522.7	$\pm 5.7$	372	$\pm 110$	-29	11.84	1.1	0.054	5	0.629	5.2	0.08446	1.1	0.22
4033-3_6.1	0.32	204	83	0.42	14.9	523.3	$\pm 4.8$	676	$\pm 110$	29	11.82	0.95	0.0621	5.4	0.723	5.4	0.08456	0.95	0.18
4033-3_7.1	0.36	175	62	0.37	12.9	526.4	$\pm 5.2$	755	$\pm 81$	44	11.75	1	0.0644	3.8	0.756	4	0.08508	1	0.26
4033-3_8.1	0.55	119	38	0.33	8.69	524	$\pm 6.3$	790	$\pm 150$	51	11.8	1.2	0.0655	7	0.765	7.1	0.0847	1.2	0.18
4033-3_9.1	0.30	190	66	0.36	13.8	522.5	$\pm 4.8$	631	$\pm 74$	21	11.84	0.96	0.0608	3.4	0.707	3.6	0.08443	0.96	0.27
4033-3_10.1	0.75	171	96	0.58	12.5	522.2	$\pm 5.4$	682	$\pm 290$	31	11.84	1.1	0.0622	14	0.724	14	0.08439	1.1	0.08
<b>Biotite plagiogranite</b>																			
2127-1.6.1	0.13	672	318	0.49	45.9	492	3.0	549	$\pm 42$	12	12.6	0.6	0.0585	1.9	0.640	2.0	0.0794	0.6	0.32
2127-1.4.1	0.00	122	31	0.26	8.62	511	5.8	645	$\pm 72$	26	12.12	1.2	0.0611	3.3	0.696	3.5	0.0825	1.2	0.33
2127-1.8.1	0.19	351	130	0.38	25	513	4.2	448	$\pm 60$	-13	12.07	0.9	0.0559	2.7	0.638	2.8	0.0828	0.9	0.30

(continued on next page)

Table 3 (continued)

Sample, point	$^{206}\text{Pb}_{\text{e}}$ , %	U ppm	T ppm	$^{232}\text{Th}/^{238}\text{U}$	$^{206}\text{Pb}^*$ , ppm	$^{206}\text{Pb}/^{238}\text{U}$	Isotopic age			Discor- dance, %	$^{238}\text{U}/^{206}\text{Pb}$ Error, $\pm\%$	$^{207}\text{Pb}^*/^{235}\text{U}$ Error, $\pm\%$	$^{206}\text{Pb}^*/^{238}\text{U}$ Error, $\pm\%$	Correlation coefficient					
							$^{207}\text{Pb}/^{206}\text{Pb}$	$^{206}\text{Pb}/^{206}\text{Pb}$	Error, $\pm\%$										
Biotite plagiogranite																			
2127-1.7.1	0.24	211	68	0.33	15.1	517	4.6	502	$\pm 73$	-3	11.97	0.9	0.0573	3.3	0.659	3.4	0.0835	0.9	0.27
2127-1.1.1	0.20	318	121	0.39	22.9	517	3.7	518	$\pm 60$	0	11.968	0.8	0.0577	2.7	0.665	2.8	0.0836	0.8	0.26
2127-1.10.1	0.23	434	108	0.26	31.3	518	3.4	525	$\pm 57$	1	11.952	0.7	0.0579	2.6	0.668	2.7	0.0837	0.7	0.25
2127-1.9.1	0.12	486	174	0.37	35.1	520	3.2	541	$\pm 42$	4	11.909	0.6	0.0583	1.9	0.675	2.0	0.0840	0.6	0.31
2127-1.3.1	0.17	335	125	0.39	24.2	521	4.3	503	$\pm 54$	-3	11.88	0.9	0.0573	2.5	0.665	2.6	0.0842	0.9	0.33
2127-1.5.1	0.00	77	38	0.51	5.65	531	7.4	532	$\pm 89$	0	11.65	1.5	0.0581	4.1	0.687	4.3	0.0858	1.5	0.34
Tannu-Ola diorite–granodiorite–plagiogranite complex																			
Hornblende diorite																			
2168-2_1.1	0.24	182	130	0.74	12.3	487	$\pm 8.3$	413	$\pm 94$	-15	12.71	1.8	0.055	4.2	0.595	4.6	0.079	1.8	0.39
2168-2_2.1	0.00	131	30	0.24	8.91	490.6	$\pm 9.1$	522	$\pm 90$	6	12.65	1.9	0.0578	4.1	0.63	4.5	0.079	1.9	0.42
2168-2_3.1	0.00	89	34	0.39	6.25	508	$\pm 10$	505	$\pm 110$	-1	12.21	2.1	0.0573	5.1	0.648	5.5	0.082	2.1	0.39
2168-2_4.1	0.30	298	141	0.49	20.2	489.3	$\pm 7.7$	402	$\pm 87$	-18	12.64	1.6	0.0548	3.9	0.595	4.2	0.079	1.6	0.39
2168-2_5.1	0.25	177	66	0.38	12	490.5	$\pm 8.5$	534	$\pm 91$	9	12.62	1.8	0.0581	4.2	0.633	4.5	0.079	1.8	0.4
2168-2_6.1	0.00	198	96	0.50	13.6	496.5	$\pm 8.3$	407	$\pm 110$	-18	12.49	1.7	0.0549	4.8	0.606	5.1	0.080	1.7	0.34
2168-2_7.1	0.00	108	43	0.41	7.43	494.2	$\pm 9.5$	405	$\pm 100$	-18	12.55	2	0.0548	4.6	0.602	5	0.08	2	0.40
2168-2_8.1	0.00	122	61	0.52	8.39	495.5	$\pm 9.3$	541	$\pm 93$	9	12.52	1.9	0.0583	4.3	0.642	4.7	0.08	1.9	0.42
2168-2_9.1	0.21	297	122	0.43	20.3	491	$\pm 7.7$	530	$\pm 70$	8	12.61	1.6	0.058	3.2	0.633	3.6	0.079	1.6	0.45
2168-2_10.1	0.43	141	55	0.40	9.53	487.2	$\pm 9.6$	409	$\pm 130$	-16	12.68	2	0.0549	5.7	0.594	6	0.079	2	0.34
Hornblende diorite																			
77-1.1	0.11	280	81	0.30	19.4	500.1	$\pm 7.2$	449	$\pm 50$	-10	12.4	1.5	0.0559	2.3	0.622	2.7	0.0807	1.5	0.55
77-2.1	0.49	71	18	0.26	4.98	505	$\pm 11$	593	$\pm 120$	17	12.26	2.2	0.0597	5.6	0.671	6	0.0815	2.2	0.37
77-3.1	0.00	394	63	0.17	27.7	507.7	$\pm 7.4$	489	$\pm 37$	-4	12.2	1.5	0.05693	1.7	0.643	2.3	0.0819	1.5	0.67
77-4.1	0.05	682	87	0.13	46.8	495.4	$\pm 6.9$	443	$\pm 31$	-11	12.52	1.4	0.05576	1.4	0.614	2	0.0799	1.4	0.72
77-4.2	0.00	86	24	0.29	5.93	498.5	$\pm 9.1$	425	$\pm 83$	-15	12.44	1.9	0.0553	3.7	0.613	4.2	0.0804	1.9	0.45
77-5.1	0.28	161	53	0.34	10.9	486.9	$\pm 7.5$	485	$\pm 82$	0	12.74	1.6	0.0568	3.7	0.615	4.1	0.0785	1.6	0.40
77-6.1	0.29	152	41	0.28	10.4	490.7	$\pm 7.9$	437	$\pm 89$	-11	12.64	1.7	0.0556	4	0.607	4.3	0.0791	1.7	0.39
77-7.1	0.09	376	54	0.15	25.7	493.2	$\pm 6.9$	503	$\pm 40$	2	12.58	1.5	0.0573	1.8	0.628	2.3	0.0795	1.5	0.63
77-8.1	0.00	279	47	0.17	19.2	497.4	$\pm 7.5$	521	$\pm 47$	5	12.47	1.6	0.0578	2.1	0.639	2.6	0.0802	1.6	0.59
77-9.1	0.00	147	26	0.18	10.1	494.7	$\pm 8.4$	515	$\pm 64$	4	12.54	1.8	0.0576	2.9	0.634	3.4	0.0798	1.8	0.52
Porphyritic plagiogranite																			
2012-2_1.1	1.08	173	54	0.32	12.3	508	$\pm 4.5$	247	$\pm 210$	-51	12.19	0.91	0.0511	9	0.578	9	0.08199	0.91	0.10
2012-2_2.1	0.72	118	36	0.31	8.3	504.7	$\pm 4.5$	456	$\pm 130$	-10	12.28	0.93	0.0561	6	0.63	6.1	0.08144	0.93	0.15
2012-2_3.1	0.76	131	40	0.32	9.33	509.5	$\pm 4.3$	390	$\pm 140$	-24	12.16	0.89	0.0544	6.4	0.617	6.5	0.08224	0.89	0.18
2012-2_4.1	0.74	127	42	0.34	8.9	503.2	$\pm 4.4$	330	$\pm 140$	-34	12.32	0.91	0.053	6.2	0.594	6.3	0.08118	0.91	0.15
2012-2_5.1	1.93	127	51	0.41	9.14	508.7	$\pm 6.6$	246	$\pm 340$	-52	12.17	1.3	0.0511	15	0.579	15	0.0821	1.3	0.09
2012-2_6.1	0.59	153	47	0.32	10.7	500	$\pm 3.9$	477	$\pm 87$	-5	12.395	0.8	0.0566	3.9	0.63	4	0.08066	0.8	0.20
2012-2_7.1	0.69	126	42	0.35	8.86	504.2	$\pm 6.6$	444	$\pm 140$	-12	12.29	1.4	0.0558	6.5	0.626	6.6	0.0814	1.4	0.21

(continued on next page)

Table 3 (continued)

Sample, point	$^{206}\text{Pb}_{\text{e}}$ %	U ppm	T ppm	$^{232}\text{Th}/^{238}\text{U}$	$^{206}\text{Pb}^*$ , ppm	$^{206}\text{Pb}/^{238}\text{U}$	$^{207}\text{Pb}/^{206}\text{Pb}$	Isotopic age $^{206}\text{Pb}/^{238}\text{U}$	Error, $^{238}\text{U}/^{206}\text{Pb}$ ± %	Discor- dance, %	$^{207}\text{Pb}^*/^{235}\text{U}$	Error, $^{207}\text{Pb}^*/^{235}\text{U}$ ± %	$^{206}\text{Pb}^*/^{238}\text{U}$	Error, $^{206}\text{Pb}^*/^{238}\text{U}$ ± %	Correlation coefficient				
<b>Porphyritic plagiogranite</b>																			
2012-2_8.1	3.44	231	154	0.69	16.9	507.8	$\pm 4.5$	369	$\pm 190$	-27	12.19	0.92	0.054	8.3	0.08196	0.92			
2012-2_9.1	0.26	109	35	0.33	7.6	502.9	$\pm 4.4$	594	$\pm 74$	18	12.32	0.91	0.0597	3.4	0.08113	0.91			
2012-2_10.1	1.46	135	39	0.30	9.55	503.1	$\pm 4.6$	206	$\pm 200$	-59	12.32	0.96	0.0502	8.4	0.08118	0.96			
<b>Porphyritic plagiogranite</b>																			
2025-1_1.1	0.20	343	142	0.43	24.7	519	$\pm 10$	494	$\pm 53$	-5	11.91	2	0.059	2.4	0.057	3.1	0.66	2	0.64
2025-1_2.1	0.00	55	23	0.43	3.82	498	$\pm 11$	597	$\pm 110$	20	12.45	2.4	0.06	4.8	0.060	5.4	0.663	2.4	0.44
2025-1_3.1	0.13	266	100	0.39	18.8	508.7	$\pm 9.7$	451	$\pm 51$	11	12.16	2	0.057	2.3	0.056	3	0.634	2	0.65
2025-1_4.1	0.53	71	36	0.53	4.82	491	$\pm 19$	415	$\pm 140$	15	12.58	4	0.059	6.1	0.055	7.3	0.601	4	0.55
2025-1_5.1	0.12	1080	335	0.32	77.3	515.9	$\pm 9.4$	494	$\pm 29$	-4	11.99	1.9	0.058	1.3	0.057	2.3	0.656	1.9	0.82
2025-1_6.1	0.47	284	143	0.52	19.8	500.1	$\pm 9.6$	540	$\pm 94$	8	12.33	2	0.062	4.3	0.058	4.7	0.648	2	0.42
2025-1_7.1	0.12	320	139	0.45	22.3	501.8	$\pm 9.5$	494	$\pm 46$	-2	12.34	2	0.058	2.1	0.057	2.9	0.637	2	0.69
2025-1_8.1	0.09	969	346	0.37	69.4	515.6	$\pm 9.4$	515	$\pm 30$	0	12	1.9	0.058	1.4	0.058	2.3	0.661	1.9	0.81
2025-1_9.1	0.40	94	44	0.49	6.75	515	$\pm 11$	557	$\pm 120$	8	11.98	2.2	0.062	5.6	0.059	6.1	0.673	2.2	0.37
2025-1_10.1	0.33	118	44	0.38	8.24	503	$\pm 10$	530	$\pm 90$	5	12.29	2.1	0.061	4.1	0.058	4.6	0.649	2.1	0.46
<b>Argilik granite-leucogranite complex</b>																			
<b>Biotite leucogranite</b>																			
2226-1_1.1	0.77	100	65	0.67	6.38	456	6.3	281	$\pm 200$	-38	13.64	1.4	0.0519	8.9	0.524	9	0.0733	1.4	0.16
2226-1_2.1	0.00	122	95	0.80	7.6	450	6.2	456	$\pm 82$	1	13.82	1.4	0.0561	3.7	0.560	3.9	0.0724	1.4	0.36
2226-1_3.1	0.68	129	82	0.65	7.89	440	6.5	284	$\pm 180$	-36	14.16	1.5	0.0520	7.9	0.506	8.1	0.0706	1.5	0.19
2226-1_4.1	0.77	124	101	0.84	7.64	442	6.2	134	$\pm 220$	-70	14.08	1.5	0.0487	9.5	0.477	9.6	0.0710	1.5	0.15
2226-1_5.1	2.48	200	135	0.70	12.7	450	5.9	632	$\pm 250$	40	13.82	1.4	0.0608	12	0.606	12	0.0723	1.4	0.12
2226-1_6.1	0.00	109	57	0.54	6.77	451	6.5	530	$\pm 84$	18	13.81	1.5	0.0580	3.8	0.579	4.1	0.0724	1.5	0.36
2226-1_7.1	0.74	107	56	0.54	6.67	449	6.0	291	$\pm 200$	-35	13.85	1.4	0.0521	8.7	0.519	8.8	0.0722	1.4	0.16
2226-1_8.1	0.00	151	104	0.71	9.49	457	4.8	528	$\pm 70$	16	13.62	1.1	0.0579	3.2	0.587	3.4	0.0734	1.1	0.32
2226-1_9.1	0.49	156	93	0.61	9.99	460	5.0	401	$\pm 130$	-13	13.52	1.1	0.0547	5.8	0.558	5.9	0.0740	1.1	0.19
2226-1_10.1	0.83	133	91	0.71	8.19	444	5.4	255	$\pm 200$	-43	14.02	1.3	0.0513	8.6	0.504	8.7	0.0713	1.3	0.15
<b>Biotite-hornblende leucogranite</b>																			
2422_6.1	0.13	260	161	0.64	16	444.6	$\pm 2.6$	511	$\pm 46$	15	14.006	0.6	0.0575	2.1	0.566	2.2	0.0714	0.6	0.27
2422_10.1	0.67	171	100	0.61	10.6	445.3	$\pm 3.4$	439	$\pm 120$	-1	13.98	0.78	0.0557	5.3	0.549	5.4	0.0715	0.78	0.15
2422_15.1	0.11	184	146	0.82	11.3	445.8	$\pm 3$	582	$\pm 47$	31	13.965	0.7	0.0594	2.2	0.587	2.3	0.0716	0.7	0.31
2422_9.1	0.06	363	262	0.74	22.4	446.2	$\pm 2.4$	495	$\pm 43$	11	13.954	0.55	0.0571	1.9	0.564	2	0.0717	0.55	0.27
2422_7.1	0.39	236	135	0.59	14.6	446.3	$\pm 2.8$	448	$\pm 69$	0	13.948	0.64	0.0559	3.1	0.552	3.2	0.0717	0.64	0.21
2422_8.1	0.00	180	94	0.54	11.1	446.4	$\pm 3$	436	$\pm 43$	-2	13.946	0.69	0.0556	1.9	0.55	2	0.0717	0.69	0.34
2422_4.1	0.17	520	271	0.54	32.2	447.3	$\pm 2$	416	$\pm 37$	-7	13.918	0.47	0.05509	1.6	0.5457	1.7	0.0718	0.47	0.28
2422_14.1	0.52	467	265	0.59	29	447.4	$\pm 2.6$	369	$\pm 63$	-17	13.913	0.6	0.054	2.8	0.535	2.9	0.0719	0.6	0.21
2422_11.1	0.00	264	131	0.51	16.3	447.6	$\pm 2.6$	545	$\pm 36$	22	13.909	0.6	0.05839	1.6	0.579	1.7	0.0719	0.6	0.35
2422_12.1	0.74	351	298	0.88	21.9	448.7	$\pm 2.5$	331	$\pm 79$	-26	13.871	0.58	0.0553	3.5	0.527	3.5	0.0721	0.58	0.17
2422_13.1	0.54	130	95	0.76	8.09	449	$\pm 4$	554	$\pm 140$	23	13.86	0.92	0.0586	6.4	0.583	6.4	0.0721	0.92	0.14

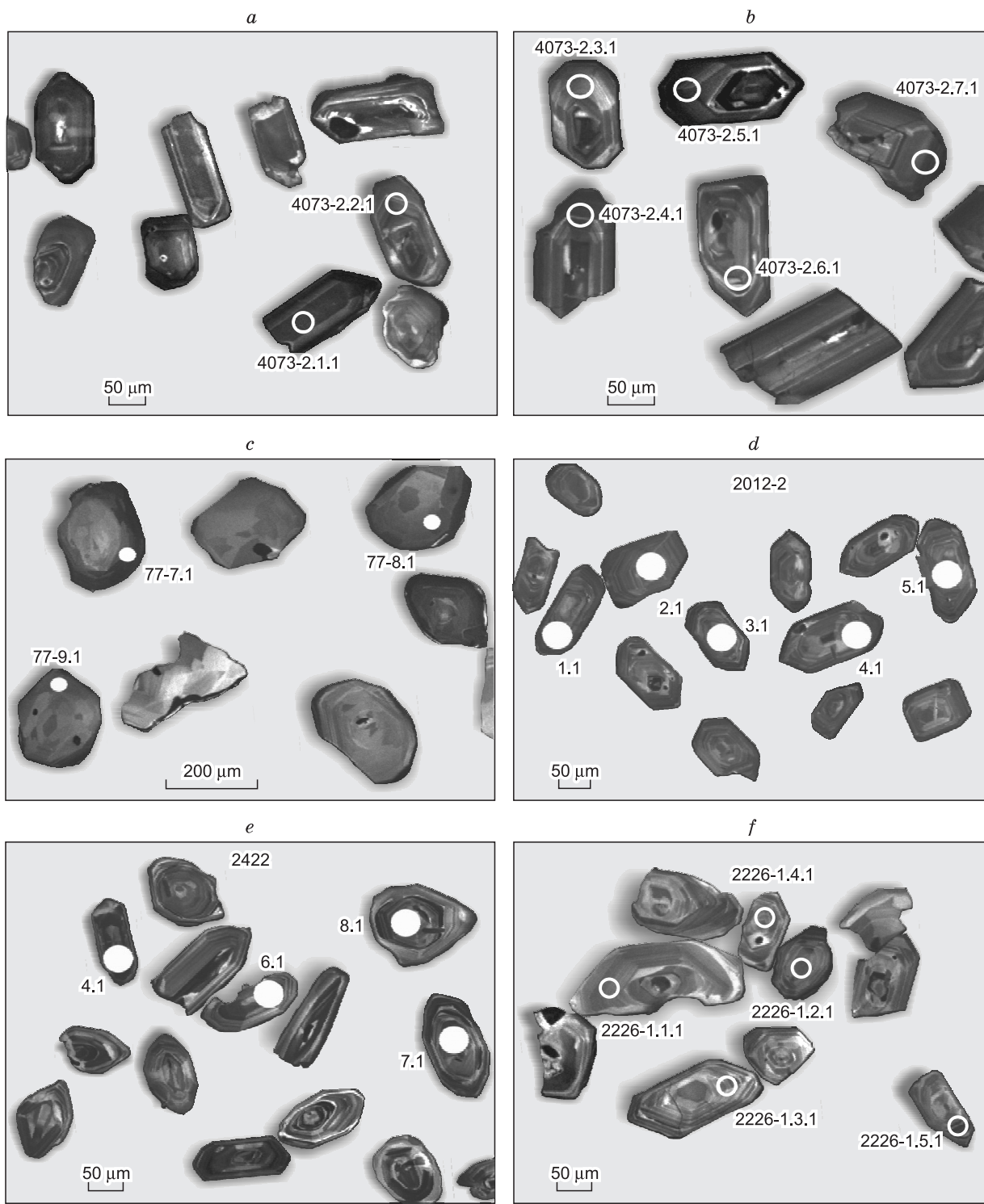


**Fig. 7.** CL photomicrographs of the internal structure of zircon crystals from the rocks of the Maina-type (*a*, *b*), Tannu-Ola (*c*, diorites, *d*, plagiogranites), and Argolik (*e*, *f*) complexes. Isotope measurement points and their numbers are shown for some grains. *a*, *b*, Zircons from porphyritic granite (sample 4073-2), *c*, zircons from hornblende diorite (sample 77), *d*, zircons from porphyritic plagiogranite (sample 2012-2), *e*, zircons from biotite-hornblende leucogranite (sample 2422), *f*, zircons from biotite leucogranite (sample 2226-1).

**Table 4.** Results of Sm/Nd and Rb/Sr studies of the Ungesh pluton granitoids

Sample	Rb	Sr	$^{87}\text{Rb}/^{86}\text{Sr}$	$^{87}\text{Sr}/^{86}\text{Sr}$	$\pm 2\sigma$	$(^{87}\text{Sr}/^{86}\text{Sr})_0$	Sm	Nd	$^{147}\text{Sm}/^{144}\text{Nd}$	$^{143}\text{Nd}/^{144}\text{Nd}$	$\pm 2\sigma$	$(^{143}\text{Nd}/^{144}\text{Nd})_0$	$\varepsilon_{\text{Nd}}(T)$	$T_{\text{Nd}}$ (DM-2st)
	ppm	ppm					ppm							
2226-1	125.8	139.9	2.601	0.720009	0.000008	0.703298	6.752	34.83	0.1172	0.512683	0.000023	0.512337	5.46	0.71
2092-1	2.391	160.7	0.043	0.704216	0.000015	0.703890	0.814	2.846	0.1729	0.512812	0.000022	0.512209	5.02	—
2422	50.55	408.6	0.3575	0.706316	0.000008	0.704040	2.139	10.85	0.1192	0.512654	0.000021	0.512305	4.74	0.78
77	18.61	580.8	0.0925	0.704214	0.000011	0.703562	2.169	9.839	0.1333	0.512725	0.000023	0.512293	5.71	0.72

Note. 2226-1, biotite leucogranite (Argolik complex); 2092-1, hornblende plagiogranite (second phase of the Maina-type complex); 2422, biotite–hornblende leucogranite (Argolik complex); 77, hornblende diorite (first phase of the Tannu-Ola complex).

Four U/Pb zircon ages (SHRIMP-II) were obtained for the rocks of the Tannu-Ola complex of the Ungesh pluton: two for hornblende diorites of the first phase (samples 77 and 2168-2) and two for plagiogranites of the second phase (samples 2012-2 and 2025-1). The dated yellow and brown zircons are transparent euhedral and subhedral prismatic crystals and isometric grains. The crystals are 130–300  $\mu\text{m}$  in average length, with an average elongation index of 1.4–2.3. They show bright CL, have sector zoning, traces of fine zoning, and random black thin rims (Fig. 7c). The concordant age was estimated from 10 measurements for zircon monofractions from each rock sample; the concordance probability is within 0.14–0.63. The morphology of zircons from the Tannu-Ola granitoids points to the middle–late Cambrian (508–492 Ma) magmatic formation of the rocks.

The results of Sm/Nd and Rb/Sr isotope studies of the hornblende diorites of the first phase of the Tannu-Ola complex (sample 77) show a high  $\varepsilon_{\text{Nd}}(T)$  value (5.71) and a low primary  $^{87}\text{Sr}/^{86}\text{Sr}$  value (0.704214) (Table 4). The model age of the rocks corresponds to the Neoproterozoic ( $T_{\text{Nd}}(\text{DM-2st}) = 0.72 \text{ Ga}$ ).

The U/Pb isotope studies of zircons from the Argolik complex were performed for two samples of leucogranites (2226-1 and 2422). The zircons are colorless transparent euhedral prismatic crystals; many of them contain reddish-brown inclusions and have cracks. The average length of the crystals is 90–270  $\mu\text{m}$ , and the average elongation index is 1.3–3.7. The zircons show bright CL and fine and sector zoning. The results obtained indicate the Late Ordovician (451–447 Ma) age of the Argolik granitoids.

The Sm/Nd and Rb/Sr isotope studies of samples 2226-1 and 2422 (Table 4) yield  $\varepsilon_{\text{Nd}}(T) = 5.46$  and 4.74 and  $^{87}\text{Sr}/^{86}\text{Sr} = 0.703298$  and 0.704040, respectively. The model age of the rocks corresponds to the Neoproterozoic ( $T_{\text{Nd}}(\text{DM-2st}) = 0.71 \text{ Ga}$  for sample 2226-1 and 0.78 Ga for sample 2422).

Thus, the geochronological U/Pb (SHRIMP II) studies of zircons from the Ungesh pluton granitoids yield the following time intervals of the rock formation: Maina-type complex, 534–518 Ma; Tannu-Ola complex, 508–492 Ma; and Argolik complex, 451–447 Ma.

## METALLOGENY OF THE GRANITOIDS COMPLEXES

The granitoid areas of the Ungesh pluton mark the border of the western part of the East Tannu-Ola ore district (ETOD) within the Tannu-Ola–Ulugoi metallogenic zone (Fig. 1). There are indicators of Au-containing polymetallic (Cu, Pb, Zn, Au, and Ag), Au, Cu, Fe, and Mo types of mineralization in the ETOD (Figs. 1 and 2). All these types are genetically related to granitoid complexes.

Polymetallic mineralization of volcanohydrothermal setting, similar to the mineralization in the Kyzyl–Tashtyg ore cluster, is related to the formation of both Maina-type granitoids and an island-arc association of early Cambrian volcanic complexes. It is not ruled out that the polymetallic ores recrystallized as a result of the intrusion of the later Ungesh pluton massifs. The intrusion of Maina-type granitoids also resulted in magnetite-containing garnet–pyroxene skarns and gold–sulfide–quartz veins. The quartz veins are single <1 m thick bodies, usually with Au < 1 ppm. It is difficult to distinguish between the gold mineralization formed at this stage and the more extensively manifested late Cambrian gold mineralization.

The ETOD gold mineralization is controlled mostly by the large Tannu-Ola complex. Gold–skarn mineralization is genetically related to the intrusion of the first-phase diorites and quartz diorites of the Tannu-Ola complex. Garnet–pyroxene skarns form small lenticular bodies up to 5–10 m in thickness and tens of meters in dip and strike length. The skarns bear not only magnetite but also chalcopyrite–bornite, quartz, and gold types of mineralization. Abundant gold–sulfide–quartz veins and veinlets are genetically related to the second-phase granitoids of the Tannu-Ola complex. The content of gold increases at the sites where vein–veinlet quartz mineralization is superposed on skarnified rocks. The large-scale occurrence of ore-forming processes is due to widely manifested magmatism, on the one hand, and to the high permeability of intensely dislocated island-arc volcanic and intrusive complexes, on the other.

In addition, the Tannu-Ola granitoids can be considered ore-generating for porphyry Mo–Cu mineralization, as in the Kyzyl–Chadr ore cluster, where porphyritic intrusions

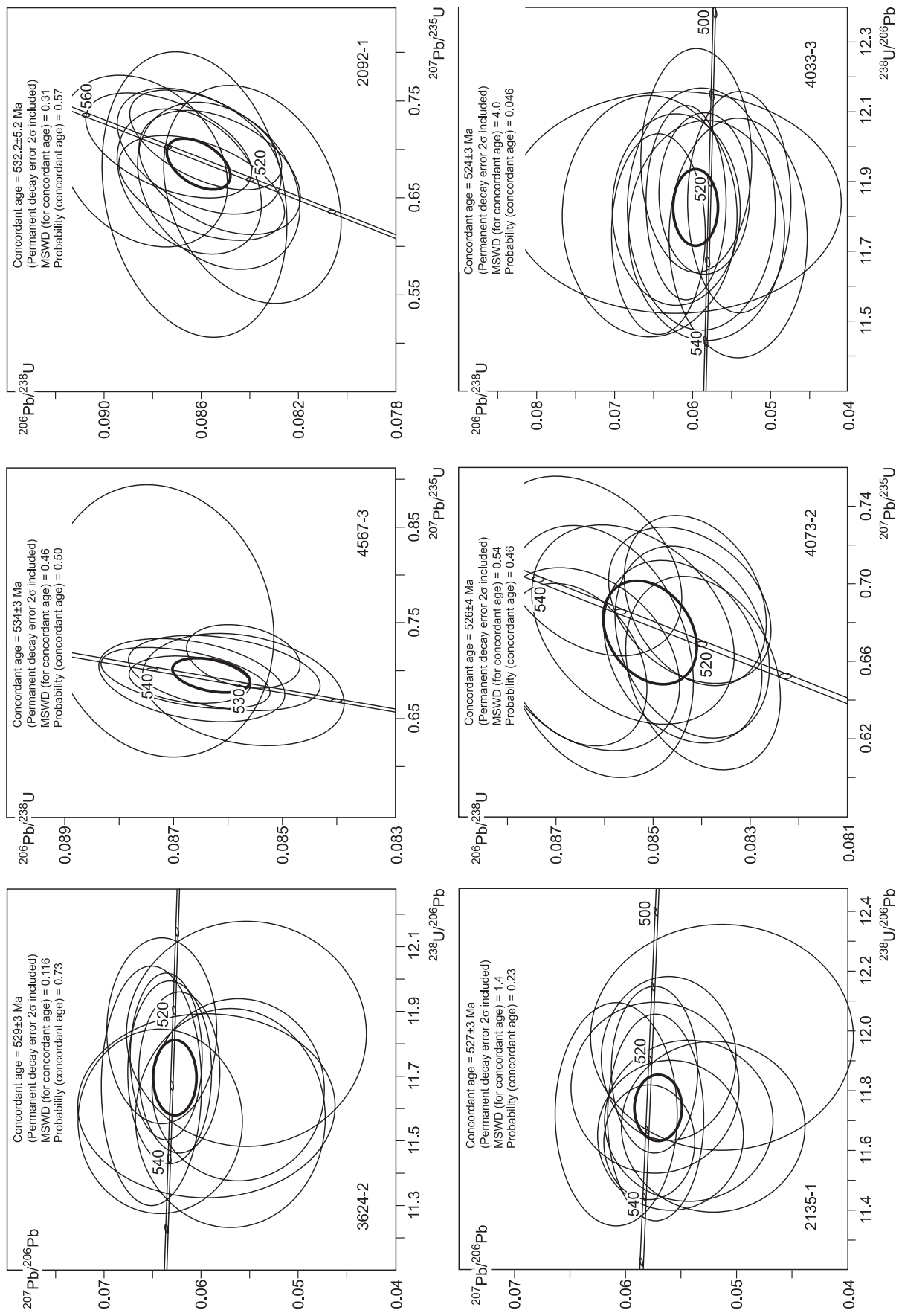


Fig. 8. U/Pb isotope concordia diagrams for zircons from the Ungesh pluton rocks. The results of analyses are given in Table 3.

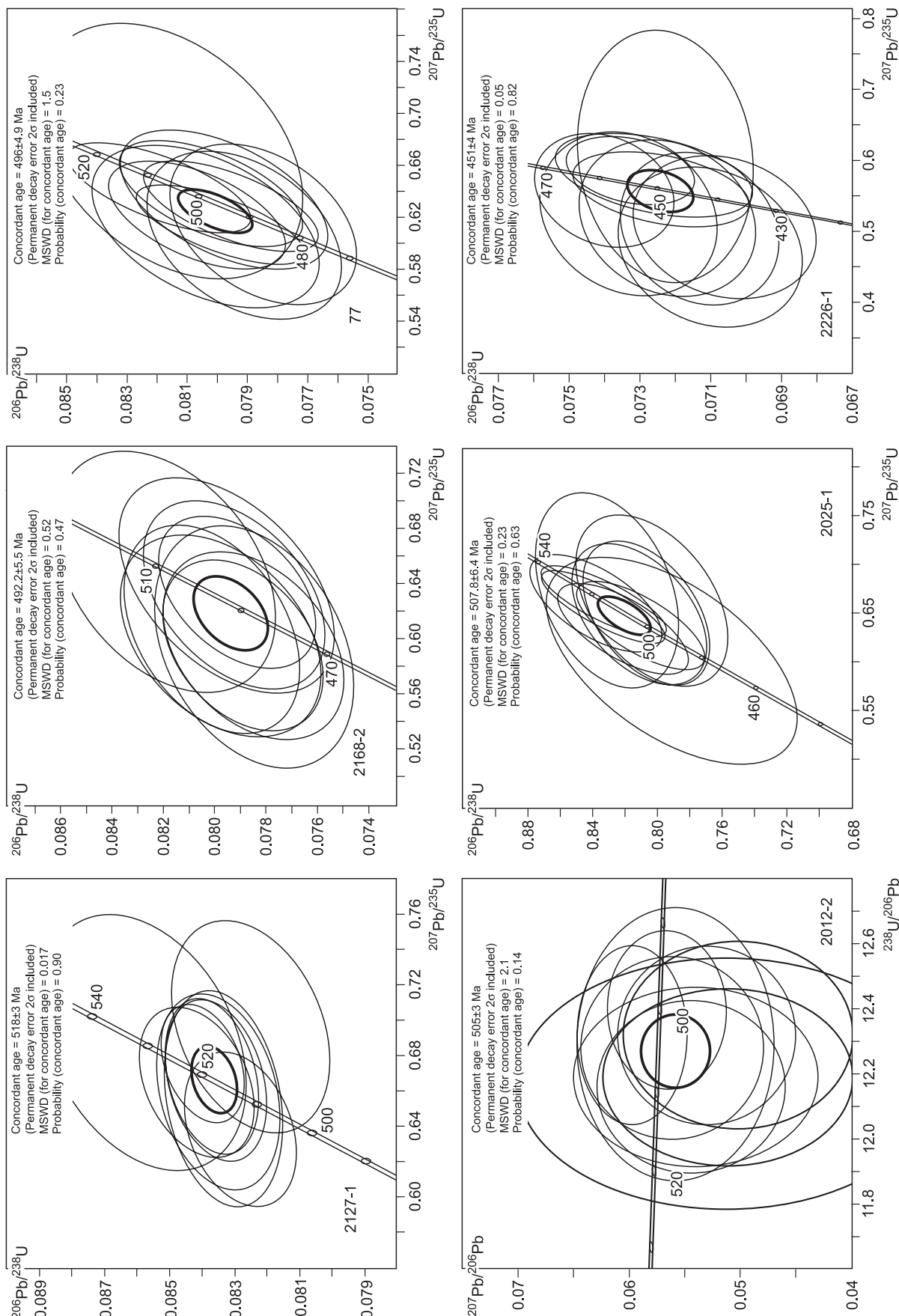


Fig. 8 (continued).

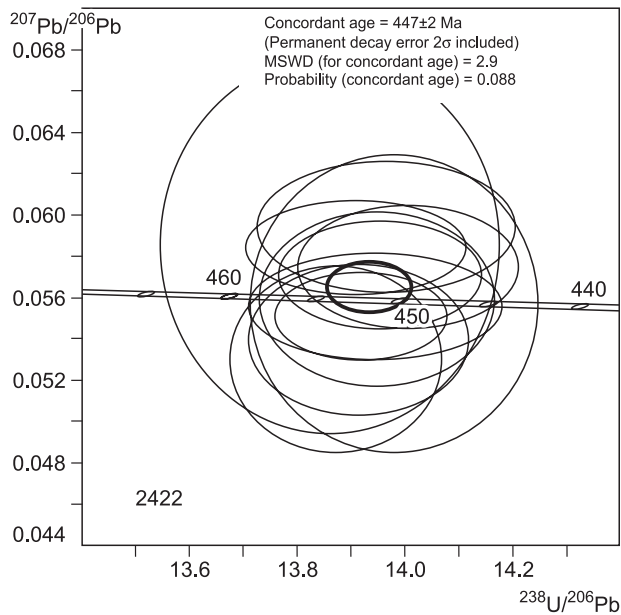


Fig. 8 (continued).

with Au–Cu mineralization are dated at  $490 \pm 4$  to  $508 \pm 7$  Ma (Gusev et al., 2014).

No gold–sulfide–quartz veins, metasomatites, or other indicators of mineralization have been found yet in the younger granitoids of the Argolik complex. The Argolik granite massifs with an age of  $447 \pm 2$  Ma (according to dating of sample 2422) break through gold-bearing skarns with gold–sulfide–quartz veinlets.

Geochemical anomalies, secondary aureoles, and dispersion trains of Cu, Mo, and Au are spatially associated with the post-ore Argolik granitoid massifs poor in ore components.

## DISCUSSION

We have established the polyformational and polychronous setting of the Ungesh pluton and have recognized massifs of three granitoid complexes. The pluton is composed mostly of the rocks of the two-phase Tannu-Ola complex. We have first revealed rocks of a two-phase complex on the pluton periphery and in xenolith blocks among the Tannu-Ola granitoids. They are similar in structure, composition, and age to the rocks of the Maina complex in West Sayan.

The early Cambrian Maina-type rocks differ little in physiography from the Tannu-Ola rocks; therefore, they can be reliably separated only by invoking the geochemical and isotope data. The Argolik granites are spatially confined to tectonic zones and usually form small massifs and “injected” bodies, which might be tongues of larger noneroded massifs.

The recognized granitoid complexes are different in petrochemical composition and are partly similar in contents of

REE and trace elements. The main difference is in contents of K and total alkalinity, which increase from older to younger granitoids. According to the alphabetic typification of rocks by petrochemical composition, the Maina-type granitoids are of *M*-type (White et al., 1979), the Tannu-Ola granitoids are *I*-type granites (Chappel and White, 1974), and the Argolik leucogranites have the parameters (Fig. 4c–e) of *A*-type granitoids formed in stabilized continental crust (Collins et al., 1982). All REE and multielement patterns (Fig. 5) show a high degree of fractionation, a negative Ta–Nb anomaly, Ti and P minima, and a Pb maximum. The  $\varepsilon_{\text{Nd}}(T)$  values (4.7–5.7) and model ages (0.71–0.78 Ga) of the protoliths of these granitoids are also close to each other. All the above geochemical characteristics suggest a common source of the granitoids of the studied complexes formed in different conditions of melt crystallization. The basic source of the granitoids was probably of subduction origin. Its features were inherited by the granitoids of all complexes and are expressed as a negative Ta–Nb anomaly in the multielement patterns. During the evolution of granitoid magmatism, there was probably a repeated intracrustal fractionation accompanied by the increase in SiO<sub>2</sub> and K<sub>2</sub>O contents in the crust (Rudnick, 1995; Luchitskaya, 2014; Kruk, 2015). The regularities of compositional changes in the granitoid complexes of different ages can be explained based on the tectonic model of the regional formation (Rudnev, 2013). According to this model, the Maina-type plagiogranites in association with the Kadvoi–Serlig basalt–andesite–rhyolite complex mark the initial stage of formation of an island arc, when both the mantle sources and the basic rocks of the oceanic basement and of the lower island-arc deposits were involved in the melting processes. The granitoids of the Tannu-Ola and Argolik complexes formed

at the early and final stages of the accretion–collision processes, respectively, which were followed by intracrustal fractionation. At the final stage of these processes, the upper part of the accretion–collision structure might have been subjected to local rifting. This might have led to the formation of granitoid magmas with within-plate geochemical characteristics.

The geochronological studies have yielded the time intervals of formation of the recognized granitoid complexes (534–518, 508–492, and 451–447 Ma), which correspond to the Early Paleozoic tectonomagmatic events in the East Tannu-Ola sector of the Tuvinian magmatic belt and agree with the age ranges of comagmatic polychronous plutons in Eastern Tuva (Rudnev, 2013; Rudnev et al., 2015).

Analysis of cartographic materials and metallogeny data on adjacent ore districts within the Tuvinian magmatic belt shows that the stage of formation of the Tannu-Ola granitoids included the most diverse and large-scale processes and thus is the most significant in terms of metallogeny. The metallogenic signatures of the Tannu-Ola intrusions are determined by the genetic relationship of Fe, Au, Cu, Pb, Zn, and Mo mineralization with this granitoid complex. However, the later granitoid massifs of the Argolik complex should be regarded as prospecting indicators, because their intrusion led to the partial regeneration and redistribution of ore matter within the earlier formed ore fields.

## CONCLUSIONS

The East Tannu-Ola sector of the Tuvinian magmatic belt includes widespread early Paleozoic granitoid massifs of different ages. The results of the comprehensive study of granitoids in the west of the Tannu-Ola areal pluton (Ungesh pluton) show that the Tannu-Ola complex has early Cambrian gabbro–plagiogranite massifs similar to the Maina complex in West Sayan. We separated them as an individual complex. The first phase of this Maina-type complex is gabbroids formed before the major phase of plagiogranite intrusion. Some researchers refer these gabbroids to the Ediacaran(?)–early Cambrian Mazhalyk dunite–pyroxenite–gabbro complex (Shapovalov, 2001; Mongush et al., 2011). The obtained dates indicate a synchronous formation of these gabbroids and the Maina-type granitoids. The analysis of the available and our new geological and isotope-geochronological data gives grounds to regard the studied massifs, earlier assigned to the Bren' complex (Pinus, 1961; Ivanova, 1963; Chuchko, 1965; Telesh, 1981; Shapovalov, 2001), as part of the Ordovician Argolik complex. Similar examples of reduction of the areas of the Tannu-Ola and Bren' complexes are known in Eastern Tuva (Rudnev et al., 2004, 2006, 2015; Rudnev, 2013).

Thus, three intrusive complexes with different formation conditions, ages, compositions, and metallogeny have been recognized within the Ungesh pluton.

The oldest (534–518 Ma) Maina-type gabbro–plagiogranite complex, for the first time recognized in the Tannu-Ola complex, and the Kadvoi–Serlig basalt–andesite–plagioryholite complex form an early Cambrian island-arc rock association. It is necessary to continue research in order to substantiate the recognition of early Cambrian Maina-type granitoids within other areal plutons in Tuva and to refine their structure and composition. Gold–polymetallic mineralization is genetically related to the postvolcanic hydrothermal activity at the island-arc stage, and magnetite-containing skarns and gold–sulfide–quartz veins and veinlets are the result of the intrusion of the Maina-type granitoids.

The middle–late Cambrian (508–492 Ma) Tannu-Ola diorite–granodiorite–plagiogranite complex formed at the initial stage of evolution of the accretion–collision system. The large-scale intrusive magmatism of this stage gave rise to magnetite-containing skarns with Cu (chalcopyrite–bornite) and Au mineralization and to numerous vein–veinlet zones with gold–sulfide–quartz mineralization. According to the available metallogeny data, porphyry Au–Mo–Cu mineralization forms in the second-phase rocks of the Tannu-Ola complex.

The smaller granite–leucogranite massifs of the Late Ordovician (451–447 Ma) Argolik complex formed at the late stage of evolution of the accretion–collision system. The intrusion of the Argolik granites seems to have contributed to the regeneration of older Cu and Au mineralization and its concentration within the earlier formed ore fields.

We thank E.D. Shabalinskaya and D.N. Shapovalov for valuable advice and permanent support during the geological work.

The research was performed in the framework of the state task at the Sobolev Institute of Geology and Mineralogy, Novosibirsk.

## REFERENCES

- Babin, G.A., Zeifert, L.L., Shchigrev, A.F., Shchigrev, A.F., Kondrashov, A.K., Korableva, T.V., Sazonov, V.A., Tereda, N.F., Chernykh, A.I., Golovina, A.G., 2006. Legend to the Altai–Sayan Sheets of the State Geological Map of the Russian Federation, Scale 1:1,000,000 (Third Edition) [in Russian]. Zapsibgeols”emka, Novokuznetsk.
- Black, L.P., Kamo, S.L., Allen, C.M., Aleinikoff, J.N., Davis, D.W., Korsch, R.J., Foudoulis, C., 2003. TEMORA 1: a new zircon standard for U–Pb geochronology. *Chem. Geol.* 200, 155–170.
- Bogatikov, O.A., Petrov, O.V., Sharpenok, L.N., 2009. Petrographic Code of Russia [in Russian]. VSEGEI, St. Petersburg.
- Bogomolov, E.S., Guseva, V.F., Turchenko, S.I., 2002. Mantle origin of the Pana Tundra layered mafic intrusion: evidence from Sm–Nd and Rb–Sr data. *Geochem. Int.* 40 (9), 855–859.
- Chappell, B.W., White, A.J.R., 1974. Two contrasting granite types. *Pacific Geol.* 8, 173–174.
- Chernykh, A.I., 2014. Distribution and prospects of exploration of gold mineralization in the East Tannu-Ola district, Republic of Tyva. *Rudy i Metally*, No. 5, 10–18.
- Chernykh, A.I., Vetrov, E.V., Pikhutin, E.A., 2017. Geologic structure and metallogeny of the western part of the East Tannu-Ola ore dis-

- trict (Republic of Tyva) (from new geochemical and isotope-geochronological data). Otechestvennaya Geologiya, No. 2, 4–21.
- Chuchko, V.N., Sarbaa, Ya.V., Averin, O.K., 1965. Geologic Structure and Mineral Resources of the Area of the Khovu-Aksy Ni-Co and Uzunoi Deposits (Sheets M-46-32-A, M-46-32-B, M-46-32-B(a,b), and M-46-32-G(a,b)) [in Russian]. Kyzyl, Tyvinskii Filial FBU “TFGI po SFO”, No. 835.
- Collins, W.J., Beams, S.D., White, A.J.R., Chappell, B.W., 1982. Nature and origin of A-type granites with particular reference to southeastern Australia. *Contrib. Mineral. Petrol.* 80, 1–2.
- De Paolo, D.J., Linn, A.M., Schubert, G., 1991. The continental crust age distribution: methods of determining mantle separation ages from Sm–Nd isotopic data and application to the southwestern United States. *J. Geophys. Res.* 96 (B2), 2071–2088.
- Faure, G., 1986. Principles of Isotope Geology. John Wiley & Sons, New York.
- Fershtater, G.B., Malakhova, L.V., Borodina, N.S., Rapoport, M.S., 1984. Eugeosynclinal Gabbro–Granitoid Series [in Russian]. Nauka, Moscow.
- Frost, B.R., Barnes, C.G., Collins, W.J., Arculus, R.J., Ellis, D.J., Frost, C.D., 2001. A geochemical classification for granitic rocks. *J. Petrol.* 42, 1771–1802.
- Gusev, N.I., Berzon, E.I., Semenov, M.I., 2014. Kyzyl-Chadr porphyry Cu deposit (Tuva): geochemistry and age of magmatism. *Regional'naya Geologiya i Metallogeniya*, No. 59, 70–79.
- Harris, N.B.W., Pearce, J.A., Tindle, A.G., 1986. Geochemical characteristics of collision-zone magmatism, in: Cowards, M.P., Ries, A.C. (Eds.), Collision Tectonics. Geol. Soc. London, Spec. Publ. 19, 67–81.
- Ivanova, T.N., 1963. Regularities of Early Paleozoic Magmatism Evolution in Different Structures in Tuva [in Russian]. Gosgeoltekhnidat, Moscow.
- Kruk, N.N., 2015. Continental crust of Gorny Altai: stages of formation and evolution; indicative role of granitoids. *Russian Geology and Geophysics (Geologiya i Geofizika)* 56 (8), 1097–1113 (1403–1423).
- Liew, T.C., Hofmann, A.W., 1988. Precambrian crustal components, plutonic associations, plate environment of the Hercynian Fold Belt of Central Europe: Indications from a Nd and Sr isotopic study. *Contrib. Mineral. Petrol.* 98, 129–138.
- Luchitskaya, M.V., 2014. Meso–Cenozoic Granitoid Magmatism and Formation of Continental Crust in the Northern Framing of the Pacific [in Russian]. GEOS, Moscow.
- Ludwig, K.R., 2003. User's Manual for Isoplot/Ex, Version 3.00. A Geochronological Toolkit for Microsoft Excel. Berkeley Geochronology Center Special Publication, Berkeley, USA.
- Mongush, A.A., Lebedev, V.I., Kovach, V.P., Sal'ninkova, E.B., Druzhkova, E.K., Yakovleva, S.Z., Plotkina, Yu.V., Zagornaya, N.Yu., Travin, A.V., Serov, P.A., 2011. The tectonomagmatic evolution of structure-lithologic complexes in the Tannu-Ola zone, Tuva, in the Late Vendian–Early Cambrian (from geochemical, Nd isotope, and geochronological data). *Russian Geology and Geophysics (Geologiya i Geofizika)* 52 (5), 503–516 (649–665).
- Pearce, J.A., Harris, N.B.W., Tindle, A.G., 1984. Trace element discrimination diagrams for the tectonic interpretation of granitic rocks. *J. Petrol.* 25, 956–983.
- Pinus, G.V., 1961. Lower Cambrian Volcanism in Tuva [in Russian]. Izd. SO AN SSSR, Novosibirsk.
- Rudnev, S.N., 2013. Early Paleozoic Granitoid Magmatism in the Altai–Sayan Folded Area and in the Lake Zone in Western Mongolia [in Russian]. Izd. SO RAN, Novosibirsk.
- Rudnev, S.N., Vladimirov, A.G., Bibikova, E.V., Teleshev, A.E., Koval'ev, P.F., 2004. Composition and age of the granitoids of the Bren' massif (Eastern Tuva), in: Petrology of Igneous and Metamorphic Complexes. Proceedings of the Russian Petrographic Conference [in Russian]. TsNTI, Tomsk, Issue 4, pp. 72–77.
- Rudnev, S.N., Babin, G.A., Vladimirov, A.G., Kruk, N.N., Shokal'sky, S.P., Borisov, S.M., Travin, A.V., Levchenkov, O.A., Terleev, A.A., Kuibida, M.L., 2005. Geologic setting, age, and geochemical model of the formation of West Sayan plagiogranitoids. *Geologiya i Geofizika (Russian Geology and Geophysics)* 46 (2), 170–187 (169–187).
- Rudnev, S.N., Vladimirov, A.G., Ponomarchuk, V.A., Bibikova, E.V., Sergeev, S.A., Matukov, D.I., Plotkina, Yu.V., Bayanova, T.B., 2006. The Kaa-Khem polychronous batholith (Eastern Tuva): composition, age, sources, and geodynamic setting. *Litosfera*, No. 2, 3–33.
- Rudnev, S.N., Serov, P.A., Kiseleva, V.Yu., 2015. Vendian-Early Paleozoic granitoid magmatism in Eastern Tuva. *Russian Geology and Geophysics (Geologiya i Geofizika)* 56 (9), 1232–1255 (1572–1600).
- Rudnick, R.L., 1995. Making continental crust. *Nature* 378, 571–578.
- Shapovalov, D.N., 2001. Legend to the Upper Yenisei Sheets of the State Geological Map of the Russian Federation, Scale 1:200,000 (Second Edition) [in Russian]. Tyvinskii Filial FBU “TFGI po SFO”, Kyzyl, No. 2401.
- Sun, S.-S., McDonough, W.F., 1989. Chemical and isotopic systematics of oceanic basalts: implications for mantle composition and processes. *Geol. Soc. London, Spec. Publ.* 42, 313–345.
- Teleshev, A.E., 1981. Relationship between the heterochronous granitoids of the Bren' pluton and the Devonian volcanic complexes in Eastern Tuva, in: Igneous Complexes in South Siberian Folded Areas [in Russian]. Nauka, Novosibirsk, pp. 63–103.
- White, A.J.R., 1979. Source of granite magmas. *Geol. Soc. Am., Abst. Prog.* 11.
- Williams, I.S., 1998. U–Th–Pb geochronology by ion microprobe, in: McKibben, M.A., Shanks III, W.C., and Ridley, W.I. (Eds.), Applications of Microanalytical Techniques to Understanding Mineralizing Processes. *Rev. Econ. Geol.* 7, 1–35.

*Editorial responsibility:* N.N. Kruk